Energy & Environmental Science

REVIEW

View Article Online
View Journal | View Issue

Cite this: *Energy Environ. Sci.*, 2015, **8**, 1660

Electrospun materials for lithium and sodium rechargeable batteries: from structure evolution to electrochemical performance

Heng-Guo Wang,[ab] Shuang Yuan,[bc] De-Long Ma,[bc] Xin-Bo Zhang[c] and Jun-Min Yan*[b]

Received 12th December 2014,
Accepted 9th March 2015

DOI: 10.1039/c4ee03912b

www.rsc.org/ees

Electrospinning has been growing increasingly versatile as a promising method to fabricate one dimensional (1D) designed architectures for lithium-ion batteries (LIBs) and sodium-ion batteries (SIBs). In this review, we have summarized almost all the progress in electrospun electrode materials for LIBs, covering the structure evolution from solid nanofibers into designed 1D nanomaterials, then 1D composites with carbon nanofibers (CNFs), and finally into flexible electrode materials with CNFs. Such a development trend in electrospun electrode materials would meet the battery technology and the strong consumer market demand for portable, ultrathin/lightweight and flexible devices. Along with the avenues of research about electrospun electrode materials for LIBs, electrospun electrode materials for SIBs are a rapidly growing and enormously promising field. As a timely overview, recent studies on electrospun SIB electrode materials are also highlighted. Finally, the emerging challenges and future developments of electrospun electrode materials are concisely provided. We hope this review will provide some inspiration to researchers over a broad range of topics, especially in the fields of energy, chemistry, physics, nanoscience and nanotechnology.

Broader context

Rechargeable batteries (*e.g.* lithium-ion batteries and sodium-ion batteries) hold great promise for environmentally friendly and economic renewable energy resources. To meet the ever-expanding demand for rechargeable batteries, it is critical to design and fabricate excellent electrode materials with rational nanostructures, especially one-dimensional nanostructures. Recently, electrospinning has become a remarkably simple, versatile and cost-effective method to fabricate one dimensional designed architectures for lithium-ion batteries and sodium-ion batteries. This review is intended to systematically discuss all the progress in electrospun electrode materials, covering the structure evolution from solid nanofibers into designed 1D nanomaterials, then 1D composites with carbon nanofibers, and finally into flexible electrodes, as well as an outlook on the next generation of flexible rechargeable batteries.

1. Introduction

The global energy crisis and environmental pollution have driven scientists and engineers to develop highly efficient and environmentally friendly methods of creating and storing renewable energy. Energy conversion and storage are considered to be ever more important in the context of the increasing global energy demand. Among the currently available energy conversion and storage technologies, rechargeable (or secondary) batteries are the most successfully tried technology that can repeatedly generate clean electricity from stored materials and reversely convert electric energy into chemical energy.[1] Currently, research efforts to develop versatile rechargeable batteries have mostly focused on two types of electrochemical devices: lithium-ion batteries (LIBs)[2,3] and sodium-ion batteries (SIBs).[4,5] LIBs offer energy densities 2–3 times higher than conventional batteries,[2] and therefore they have received intense attention from both the academic community and industry as the dominant power source in hybrid electric vehicles (HEVs), plug-in hybrid electric vehicles (PHEVs), and full electric vehicles (EVs).[6] However, their power density is relatively low because of a large polarization at high charge–discharge rates.[7] On the other hand, SIBs have attracted great attention particularly in large-scale and long-term

[a] *School of Materials Science and Engineering, Changchun University of Science and Technology, Changchun 130022, China*
[b] *Key Laboratory of Automobile Materials, Ministry of Education, Department of Materials Science and Engineering, Jilin University, Changchun 130022, China. E-mail: junminyan@jlu.edu.cn*
[c] *State Key Laboratory of Rare Earth Resource Utilization, Changchun Institute of Applied Chemistry, Chinese Academy of Sciences, Changchun 130022, China*

electric energy storage applications for renewable energy and smart grids because of the huge abundance of sodium resources and low cost.[8–23] Indeed, where gravimetric energy density is not the primary concern, SIBs can be preferable to their Li-ion counterparts. Given the ever-growing demand for advanced batteries, developing low cost and high-energy and -power density batteries is of great importance. To achieve high energy and power density, it is important to design and fabricate functional nanomaterials that provide a high active surface area and an open shortened diffusion path for ionic transport and electronic conduction.

One-dimensional (1D) nanomaterials have been recognized as the most desirable material for applications in energy-related systems. Their unique structure provides an enhanced surface-to-volume ratio, short transport lengths for ionic transport and efficient 1D electron transport along the longitudinal direction. At present, these 1D nanomaterials can be prepared by a template-directed method,[24] vapor-phase approach[25] solution–liquid–solid technique,[26] solvothermal or hydrothermal synthesis,[27] self-assembly,[28] and electrospinning. As a remarkably simple, versatile and cost-effective industry-viable technology, electrospinning has been used for many years to generate 1D fibers in a continuous process, at long length scales and with controllable morphology and compositions.[29–59] More importantly, besides the relatively high production rate and simplicity of

Heng-Guo Wang

Heng-Guo Wang received his PhD degree in 2011 from Jilin University. From 2011 to 2013, he worked at Changchun Institute of Applied Chemistry as a Postdoctoral Research Associate. Currently Dr Wang is an Associate Professor at the School of Materials Science and Engineering at Changchun University of Science and Technology. His research interests focus on advanced functional nanomaterials, and their applications in energy storage and conversion fields, such as lithium-ion batteries, sodium-ion batteries, and supercapacitors.

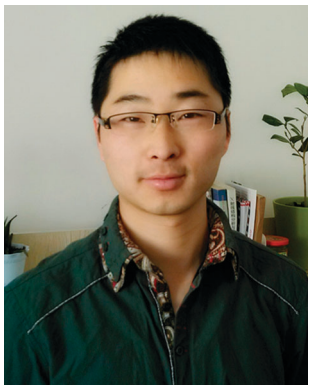

Shuang Yuan

Shuang Yuan received his Master degree in Condensed Matter Physics from Northeastern University of China in 2012. He is currently pursuing his PhD in Materials Science at Jilin University of China. His current interests include the design, synthesis and characterization of novel and advanced materials for room temperature sodium-ion batteries.

De-Long Ma

De-Long Ma received his PhD degree in 2014 from Jilin University. Currently Dr Ma is a Postdoctoral researcher at Beijing University of Technology. He is current working on the design and synthesis of nano-materials for Li-ion and Na-ion batteries.

Xin-Bo Zhang

Dr Xin-Bo Zhang (1978) joined Changchun Institute of Applied Chemistry (CIAC) as a professor of the "Hundred Talents Program" of the Chinese Academy of Sciences (CAS) in the spring of 2010. He received his PhD degree in inorganic chemistry from CIAC and was granted the CAS Presidential Scholarship Award in 2005. Then, during 2005–2010, he worked as a JSPS and NEDO fellow at the National Institute of Advanced Industrial Science and Technology (Kansai Center), Japan. His interests mainly focus on functional inorganic materials for energy storage and conversion in fuel cells and batteries, especially lithium–air batteries.

Jun-Min Yan

Dr Jun-Min Yan received her PhD degree in inorganic chemistry from Changchun Institute of Applied Chemistry, Chinese Academy of Sciences in 2006. After that, she worked as a JSPS and NEDO fellow at the National Institute of Advanced Industrial Science and Technology, Japan. At the beginning of 2010, she joined the Department of Materials Science and Engineering at Jilin University as a professor of "New Century Excellent Talents in Universities of Ministry of Education of China". Her current research interests focus on the development of new functional materials for (renewable) energy storage and conversion applications.

the setup, the electrospun nanofibers possess extremely high surface to volume ratios because of their superlong lengths and the porous substructure that is formed during the annealing process.[37]

There have already been several excellent reviews devoted to electrospun materials for energy-related applications,[60–63] even LIBs.[64,65] This review is not intended to be a comprehensive overview of electrospun materials for LIBs. Rather, we discuss a range of examples to demonstrate the design and fabrication of the unique morphology and structure prepared using electrospun technology and illustrate their significant contributions to the morphological variation and structure evolution in the study of LIBs. Our other main contribution in this work is to focus on electrospun materials for SIBs. Recently, there has been a great surge in developing room-temperature stationary SIBs for large-scale electric energy storage, and a large number of electrospun electrode materials for SIBs are already receiving increasing attention. However, to the best of our knowledge, there is no comprehensive review focusing on electrospun materials for sodium-ion batteries up to now. Thus, a review article about this topic is timely. We have tried our best to minimize the omission of relative literature, but inevitably we may miss many contributions, for which we apologize.

2. Principle of electrospinning

A schematic diagram of the fundamental setup for electrospinning is shown in Fig. 1. The conventional electrospinning setup is mainly composed of a high voltage power supply, a spinneret with a metallic needle and syringe pump, and a grounded collector (typically a metal plate or a rotating mandrel). In a typical electrospinning process, a visco-elastic precursor solution is loaded into the spinneret and fed through a syringe pump. When a voltage is applied between the spinneret and the collector, the interactions of the repulsive force developed in the precursor solution with its surface tension causes the pendant droplet to elongate, deforming into a conical structure called the Taylor cone. As the applied voltage surpasses the critical value, the repulsive electrostatic forces overcome the surface tension and a charged jet of the solution is then ejected from the tip of the Taylor cone. Then the unstable jet is elongated and whipped continuously by electrostatic repulsion until it is deposited onto the grounded collector, which results in the evaporation of the solvent and the formation of solidified continuous, ultra-thin fibres on the surface of the collector.[66–68]

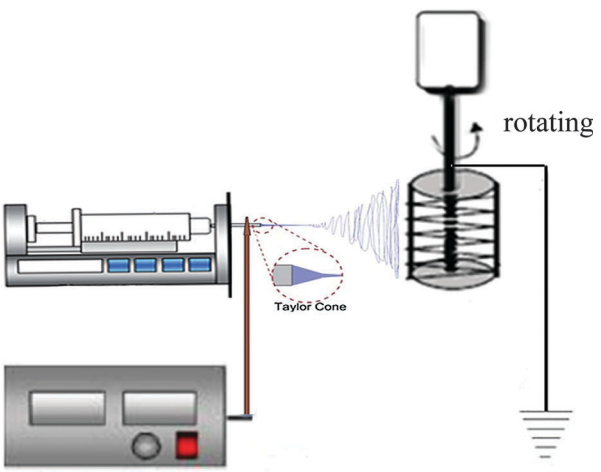

Fig. 1 Scheme of a fundamental electrospinning set-up.

The first description of apparatus for this electrospinning technique traces its roots back to an initial patent by Formhals in 1934.[69] However, the technique did not receive much attention until the 1990s. After that, several research groups (especially that of Reneker)[70,71] made a great contribution to this technique and found that it could be used to generate nanofibers from a series of different polymers. Since then, more than one hundred kinds of natural and synthetic polymers have been electrospun into nanofibers, including water-soluble polymers, such as polyvinyl alcohol (PVA), poly(vinyl pyrrolidone) (PVP), polyethylene oxide (PEO), and polyacrylamide (PAAm), and non-water-soluble polymers, such as polyacrylonitrile (PAN), polyimide (PI), poly(vinylidene fluoride) (PVDF), polylactic acid (PLA), polymethacrylate (PMMA), polystyrene (PS), polyvinylchloride (PVC), and pitch.[31,72] Generally speaking, these electrospun polymer nanofibers are usually smooth solid fibers. With the development of materials science and nanoscience, pure solid fibers and irregular arrangements cannot satisfy the application in many aspects. Thus, more and more work has focused on the optimization of the electrospinning process parameters, including the nature of the polymer solution, viscosity, voltage, and the flow rate, to obtain some special arrangements or morphologies. Among these process parameters, viscosity and voltage can play crucial roles in the morphology. In general, low viscosity and voltage are favorable for the formation of spheres or sphere and fiber composites rather than fibers. This formation process of spheres can be termed as electrospray. For example, Wang and coworkers fabricated polymer materials with controllable morphologies, such as micro- and nanofibers, spheres, cup-like, and ring-like by changing the processing parameters.[73] In addition to the fact that the process parameters can affect the morphology, the improved design or additional set up allows the preparation of core–shell, hollow, porous or multichannel structures. For example, Greiner and co-workers used coaxial electrospinning to prepare core–sheath polymer nanofibers.[74] In addition to electrospun polymer nanofibers, ceramic nanofibers and carbon nanofibers can also be prepared by electrospinning. Ceramic nanofibers prepared by electrospinning were first reported in 2002,[75,76] and since then, this approach has been greatly expanded to produce ceramic or metal oxide nanofibers from more than one hundred different materials. Herein, it should be stressed that the electrospinning method used for preparing ceramic nanofibers is different from the conventional electrospinning method used for preparing polymer nanofibers. In order to remove the polymer and prompt the formation of the ceramic or metal oxides, researchers combine the conventional electrospinning and calcination steps to prepare nanomaterials with controllable morphologies. For the electrospinning part, as mentioned above, the diameters, morphology (such as spheres or fibers) and

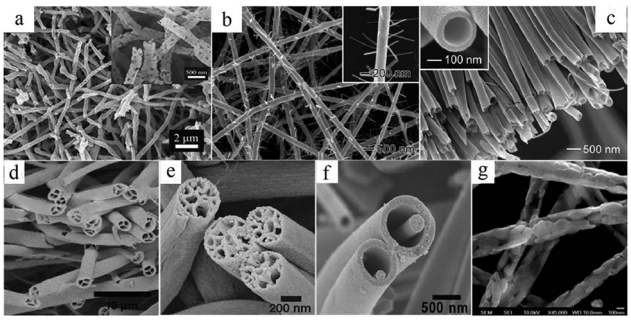

Fig. 2 Electrospun metal oxide nanofibers with designed and controllable morphologies: (a) porous V_2O_5 nanotubes,[77] (b) hierarchical V_2O_5–TiO_2–Ta_2O_5 nanofibers,[78] (c) hollow TiO_2 nanofibers,[79] (d) multichannel TiO_2 microtubes,[80] (e) porous TiO_2 nanofibers,[81] (f) nanowire-in-microtube TiO_2 fibers,[82] and (g) mesoporous V_2O_5 nanofibers.[83]

structure (such as core–shell, hollow, porous or multichannel) can be facilely controlled by simply changing the electrospinning parameters (such as viscosity, voltage or flow rate) or improving the electrospinning setup (such as using a single-spinneret or multi-spinneret).[70–74] For the calcination part, the crystallinity or designed structure (such as porous, hollow, core–sheath or hierarchical) can be facilely controlled by simply changing the calcination parameters (such as temperature or time) or precursor parameters (such as composition or additive).[75–83] Hence, electrospinning has been growing as an increasingly versatile method to fabricate various designed architectures (Fig. 2). Furthermore, carbon nanofibers (CNFs) can also be prepared by calcining the fibers electrospun from different types of precursor polymers, such as PAN, PI, PVA, PVDF, and pitch. It is well known that these designed and controllable structures are often required for rechargeable batteries, especially for LIBs. Therefore, electrospinning has become an important, popular and effective technique to prepare electrode materials for LIBs. Table 1 shows some typical examples of electrospun nanomaterials with controllable morphologies for LIBs. Tables 2 and 3 briefly describe the electrode materials based on electrospun CNFs for LIBs.

3. Electrospun nanomaterials in lithium-ion batteries

Undoubtedly, lithium-ion batteries (sometimes abbreviated to Li-ion batteries) have attracted much research attention due to their high energy density, low gravimetric density, long cycle life and lack of memory effect. Indeed, LIBs have established a strong market position, especially for portable electronic devices since they were first commercialized in the early 1990s. At present, most commonly used electrode materials for commercial LIBs are based on powder materials, such as graphite as the anode and lithium metal oxide as the cathode. However, these powder materials have long diffusion pathways for the lithium ions. This may result in the low rate performance and large volume expansion occurring during cycling, which may result in the poor cycling stability. An important approach to mitigate/resolve the problems is to employ advanced nanostructured materials with designed morphologies. Electrospinning has been recognized

Table 1 Electrochemical performance of designed electrospun nanomaterials

Materials	Structure	Performance	Rates	Ref.
SnO_2	Nanofiber	446 mA h g^{-1} after 50 cycles	100 mA g^{-1}	84
CuO	Nanofiber	425 mA h g^{-1} after 100 cycles	100 mA g^{-1}	85
$ZnFe_2O_4$	Nanofiber	733 mA h g^{-1} after 30 cycles	60 mA g^{-1}	86
$Zn_{1-x}Mn_xFe_2O_4$	Nanofiber	612 mA h g^{-1} after 50 cycles	60 mA g^{-1}	87
$Li_2ZnTi_3O_8$	Nanofiber	223.7 mA h g^{-1} after 10 cycles	22.7 mA g^{-1}	88
Ag or Au–TiO_2	Nanofiber	*ca.* 150 mA h g^{-1} after 50 cycles	33 mA g^{-1}	89
V_2O_5	Ultralong nanofiber	201 mA h g^{-1} after 50 cycles	30 mA g^{-1}	90
V_2O_5	Nanofiber	228 mA h g^{-1} after 50 cycles	35 mA g^{-1}	91
Al-intercalated V_2O_5	Nanofiber	>150 mA h g^{-1} after 50 cycles	35 mA g^{-1}	92
Nb_2O_5	Nanofiber	*ca.* 213 mA h g^{-1} after 60 cycles	50 mA g^{-1}	93
TiO_2	Nanofiber	188 mA h g^{-1} after 100 cycles	40 mA g^{-1}	94
$Li_4Ti_5O_{12}$	Nanofiber	*ca.* 135 mA h g^{-1} after 50 cycles	16 mA g^{-1}	95
$LiCoO_2$	Nanofiber	123 mA h g^{-1} after 20 cycles	20 mA g^{-1}	96
$Li_{1.2}Ni_{0.17}Co_{0.17}Mn_{0.5}O_2$	Nanofiber	*ca.* 169 mA h g^{-1} after 60 cycles	14.3 mA g^{-1}	97
Fe_2O_3	Nanorod	1095 mA h g^{-1} after 50 cycles	50 mA g^{-1}	98
NiO	Porous nanofiber	638 mA h g^{-1} after 50 cycles	40 mA g^{-1}	99
NiO–ZnO	Porous nanofiber	949 mA h g^{-1} after 120 cycles	200 mA g^{-1}	100
SnO_2	Porous nanotube	808 mA h g^{-1} after 50 cycles	180 mA g^{-1}	101
$CaSnO_3$	Porous nanotube eggroll	565 mA h g^{-1} after 50 cycles	60 mA g^{-1}	102
$CaSnO_3$	Nanotube	648 mA h g^{-1} after 50 cycles	60 mA g^{-1}	103
$ZnCo_2O_4$	Porous nanotube	1454 mA h g^{-1} after 30 cycles	100 mA g^{-1}	104
V_2O_5	Porous nanotube	105.6 mA h g^{-1} after 250 cycles	2 A g^{-1}	77
Nitridated TiO_2	Hollow nanofiber	156 mA h g^{-1} after 100 cycles	0.2 C	105
TiO_2 or TiO_2–Ag	Hollow fiber	*ca.* 100 mA h g^{-1} after 52 cycles	1 C	106
$TiNb_2O_7$	Nano-pearl-string	250 mA h g^{-1} after 50 cycles	387 mA g^{-1}	107
$LiCoO_2$–MgO	Core–shell fiber	163 mA h g^{-1} after 40 cycles	20 mA g^{-1}	108
β-$Ag_{0.33}V_2O_5$	Nanorod	180 mA h g^{-1} after 30 cycles	20 mA g^{-1}	109
MoO_2-modified TiO_2	Nanofiber	514.5 mA h g^{-1} after 50 cycles	0.2 C	110
Co_3O_4–TiO_2	Hierarchical fiber	632.5 mA h g^{-1} after 480 cycles	200 mA g^{-1}	111

Table 2 Electrochemical performance of electrospun 1D composites with CNFs

Material	Performance	Rates	Ref.
Hollow carbon nanospheres in CNFs	410 mA h g^{-1} after 300 cycles	2.2 C	112
Hollow carbon nanospheres in CNTs	330 mA h g^{-1} after 650 cycles	3.7 A g^{-1}	113
Sn in porous multichannel CMTs	648 mA h g^{-1} after 140 cycles	100 mA g^{-1}	114
Sn in bamboo-like hollow CNFs	737 mA h g^{-1} after 200 cycles	495 mA g^{-1}	115
Co–Sn alloy/CNFs	560 mA h g^{-1} after 80 cycles	161 mA g^{-1}	116
Plum-branch-like SnO_2–CNFs	539.4 mA h g^{-1} after 30 cycles	100 mA g^{-1}	117
Ultra-uniform SnO_x–CNFs	608 mA h g^{-1} after 200 cycles	500 mA g^{-1}	118
Ni-added SnO_2–CNFs	447.6 mA h g^{-1} after 100 cycles	100 mA g^{-1}	119
Uniform TiO_2–CNFs	206 mA h g^{-1} after 100 cycles	30 mA g^{-1}	120
Porous TiO_2–CNFs	680 mA h g^{-1} after 250 cycles	100 mA g^{-1}	121
Porous Co_3O_4–CNFs	534 mA h g^{-1} after 20 cycles	100 mA g^{-1}	122
MoO_2–CNFs	762.7 mA h g^{-1} after 100 cycles	50 mA g^{-1}	123
MoO–CNFs	575 mA h g^{-1} after 200 cycles	1000 mA g^{-1}	124
γ-Fe_2O_3–CNFs	837 mA h g^{-1} after 40 cycles	50 mA g^{-1}	125
Fe_3O_4–CNFs	1000 mA h g^{-1} after 80 cycles	200 mA g^{-1}	126
Si–CNFs	750 mA h g^{-1} after 40 cycles	0.33 C	127
Si–CNFs	502 mA h g^{-1} after 50 cycles	50 mA g^{-1}	128
Porous Si–CNFs	*ca.* 1104 mA h g^{-1} after 100 cycles	500 mA g^{-1}	129
Si–CNFs core–shell fibers	590 mA h g^{-1} after 50 cycles	50 mA g^{-1}	130
Si–CNFs core–shell fibers	>1250 mA h g^{-1} after 300 cycles	2750 mA g^{-1}	131
Si–CNFs–hollow graphitized carbon	1601 mA h g^{-1} after 50 cycles	100 mA g^{-1}	132
Si–TiO_2–CNFs	720 mA h g^{-1} after 55 cycles	48 mA g^{-1}	133
Uniform $Li_4Ti_5O_{12}$–CNFs	*ca.* 150 mA h g^{-1} after 100 cycles	30 mA g^{-1}	134
$Li_4Ti_5O_{12}$–CNFs	141 mA h g^{-1} after 20 cycles	0.1 C	135
$LiFePO_4$/C submicrofibers	*ca.* 125 mA h g^{-1} after 500 cycles	5 C	136
Single-crystalline $LiFePO_4$/C nanowires	146 mA h g^{-1} after 100 cycles	0.1 C	137

Table 3 Electrochemical performance of electrospun flexible electrode materials with CNFs

Material	Performance	Rates	Ref.
Porous CNFs	434 mA h g^{-1} after 50 cycles	50 mA g^{-1}	138
CNTs	454 mA h g^{-1} after 50 cycles	50 mA g^{-1}	139
Porous CNFs	454 mA h g^{-1} after 10 cycles	50 mA g^{-1}	140
Activated CNFs	385 mA h g^{-1} after 10 cycles	100 mA g^{-1}	141
Cu–CNFs	425 mA h g^{-1} after 50 cycles	50 mA g^{-1}	142
Ni–CNFs	540 mA h g^{-1} after 50 cycles	50 mA g^{-1}	143
SnO_2–CNFs core–sheath	540 mA h g^{-1} after 100 cycles	50 mA g^{-1}	144
SnO_2–CNFs	470 mA h g^{-1} after 100 cycles	50 mA g^{-1}	145
MnO_x–CNFs	433 mA h g^{-1} after 100 cycles	50 mA g^{-1}	146
MnO_x–porous CNFs	597 mA h g^{-1} after 100 cycles	50 mA g^{-1}	147
MnO_x–porous CNFs	597 mA h g^{-1} after 100 cycles	50 mA g^{-1}	148
Si–CNFs	773 mA h g^{-1} after 20 cycles	100 mA g^{-1}	149
Si–porous CNFs	630 mA h g^{-1} after 30 cycles	200 mA g^{-1}	150
Si–porous CNFs	726 mA h g^{-1} after 40 cycles	50 mA g^{-1}	151
$LiFePO_4$–CNFs	141 mA h g^{-1} after 50 cycles	17 mA g^{-1}	152
$LiFePO_4$–CNT–CNFs	169 mA h g^{-1} after 50 cycles	8.5 mA g^{-1}	153
Si–hollow carbon tubes	1000 mA h g^{-1} after 200 cycles	1000 mA g^{-1}	154
CNFs	—	—	155
Sn–CNFs	450 mA h g^{-1} after 30 cycles	25 mA g^{-1}	156
TiO_2–porous CNFs	*ca.* 400 mA h g^{-1} after 30 cycles	25 mA g^{-1}	157
Nitrogen-doped CNFs	*ca.* 530 mA h g^{-1} after 50 cycles	30 mA g^{-1}	158
Sn–CNFs	382 mA h g^{-1} after 20 cycles	0.5 mA cm^{-2}	159
Ge–CNFs	1420 mA h g^{-1} after 100 cycles	243 mA g^{-1}	160
C–SnO_2–C core–shell–shell nanofibers	837 mA h g^{-1} after 200 cycles	79 mA g^{-1}	161
Sn–SnO_x–CNFs	510 mA h g^{-1} after 40 cycles	30 mA g^{-1}	162
SnO_x–CNFs	674 mA h g^{-1} after 100 cycles	500 mA g^{-1}	163
MnO_x–CNFs	646.6 mA h g^{-1} after 50 cycles	50 mA g^{-1}	164
CoO–CNFs	633 mA h g^{-1} after 52 cycles	100 mA g^{-1}	165
MoS_2–CNFs	1150 mA h g^{-1} after 100 cycles	50 mA g^{-1}	166
$LiFe_{1-y}Mn_yPO_4$–CNFs	125 mA h g^{-1} after 75 cycles	0.5 C	167

as a simple and effective method to generate various 1D nanomaterials, which could provide an enhanced surface-to-volume ratio for the electrode–electrolyte interface, short transport lengths for ionic transport and efficient 1D electron transport along the longitudinal direction when compared to the powder materials. Also, electrospinning could be used to fabricate porous, hollow and core–sheath structured metal oxides, which could provide copious void space to accommodate the huge volume change during charge–discharge cycling, therefore efficiently improving the performance of the electrode materials. In this regard, the

versatility of electrospinning makes it highly suitable to prepare electrode materials for LIBs. In this section, recent advances in the areas of electrospun solid nanofibers, designed 1D nanomaterials, 1D composites with CNFs and flexible electrodes with CNFs for LIBs will be described.

3.1. Electrospun solid nanofibers

Recent years have witnessed a growing development of various electrospun metal oxide nanofibers for anodes in LIBs. Also, the possible formation mechanism has been proposed. For example, Teh *et al.*[86] synthesized electrospun $ZnFe_2O_4$ nanofibers as anode materials for LIBs. They demonstrated that the precursor viscosity could affect the formation of the electrospun $ZnFe_2O_4$ nanofibers or $ZnFe_2O_4$ nanorods (Fig. 3). As mentioned above, sintering the electrospun polymer–inorganic salt composite not only removes the polymer but also crystallizes the $ZnFe_2O_4$ nanoparticles. Therefore, the weight ratio of the polymer (viscosity) in the precursor is the important and determining factor. An increased weight ratio of the polymer results in the incompact dispersion of the $ZnFe_2O_4$ nanoparticles that tend to break into shorter nanorods. On the contrary, a reduced amount of the polymer helps to construct long continuous fibers. Benefiting from the functional nanostructured architecture, the nanofiber exhibits a high initial discharge capacity of 1292 mA h g^{-1} and retains a reversible capacity of 733 mA h g^{-1} up to 30 cycles at a current density of 60 mA g^{-1}, compared to nanorods with a capacity of *ca.* 200 mA h g^{-1}. The improved electrochemical performance could be attributed to the continuous 1D framework, which demonstrates the superiority of electrospun solid nanofibers. For this reason, a wide variety of metal oxide solid nanofibers have been studied by easily changing the electrospinning precursor (Table 1).

In order to achieve a better electrochemical performance, researchers have investigated controlling the compositions to overcome the disadvantages of transition metal oxides. On the one hand, transition metal oxides suffer from a high working voltage (~2.1 V *versus* Li/Li^+). To reduce the working voltage, transition metal oxide spinels (AB_2O_4) with two or more transition metal elements have been constructed. For example, constructing ternary $ZnFe_2O_4$ electrospun nanofibers by substituting Zn into Fe_2O_3 could show lower working voltages of ~1.5 V, thus effectively improving the total output voltage. Moreover, the environmentally friendly $ZnFe_2O_4$ generates a high capacity as it implements both conversion and alloy/dealloy reactions, simultaneously.[2,3] Following the beneficial effect of ternary $ZnFe_2O_4$ electrospun nanofibers, Teh *et al.*[87] further investigated the electrochemical properties of the mixed transition metallic oxide $Zn_{1-x}Mn_xFe_2O_4$ nanofibers by replacing Zn with Mn and found that the replacement not only successfully brought down the working voltage, but also improved the capacity. On the other hand, transition metal oxides also suffer from poor electrical conductivity. One of the strategies proposed to overcome these drawbacks is the incorporation of metal nanoparticles, which can improve the electrical conductivity of electrodes through the formation of a conductive percolation network. For example, Nam *et al.*[89] introduced metallic nanoparticles (Ag or Au) into TiO_2 nanofibers and showed that the embedded metallic NPs could promote lithium-ion diffusion and charge transfer. In particular, their specific capacity was improved by 20% or more and the rate performance was improved 2-fold compared to bare TiO_2 nanofibers. Therefore, achieving an improvement in the anode performance by means of the electrospun nanofibers is feasible.

Vanadium pentoxide (V_2O_5) is one of the multi-electron battery materials and has a high theoretical capacity. Since the reversible multi-electron electrochemical lithium-ion intercalation in V_2O_5 was first reported in 1976 by Whittingham,[168–170] intense interest has been focused on applying V_2O_5 as a cathode material for rechargeable LIBs. Unfortunately, until now, its practical application in rechargeable LIBs has been seriously hindered by its poor structural stability, low electronic conductivity, and sluggish electrochemical kinetics.[171] To overcome these problems, the use of electrospinning to prepare high-surface-area 1D V_2O_5 nanostructures is feasible. For example, Mai *et al.*[90] prepared ultralong hierarchical vanadium oxide nanowires constructed from attached vanadium oxide nanorods (Fig. 4). At a current rate of 30 mA g^{-1}, its initial discharge capacities were up to 275 and 390 mA h g^{-1} and the 50th discharge capacities were 187 and 201 mA h g^{-1} in the voltage range 2.0–4.0 and 1.75–4.0 V, respectively. Interestingly, compared with self-aggregated short nanorods synthesized by hydrothermal methods, the unique nanorod-in-nanowire structures exhibit a much higher capacity. This study highlights once again the importance of the continuous 1D framework of electrospun nanofibers to avoid the self-aggregation of short nanorods, thus enhancing the effective contact areas of active materials, conductive additives, and electrolytes. The use of single-phase, polycrystalline and high aspect ratio V_2O_5 nanofibers could also improve the electrochemical performance, especially in terms of the cycling stability.[91] Furthermore, the incorporation of transition metal cations like Al^{3+} and Ag^+ into V_2O_5 layers could enhance the structural stability during Li-intercalation/deintercalation due to the formation of $[MO_6]$ octahedral units.[172–176]

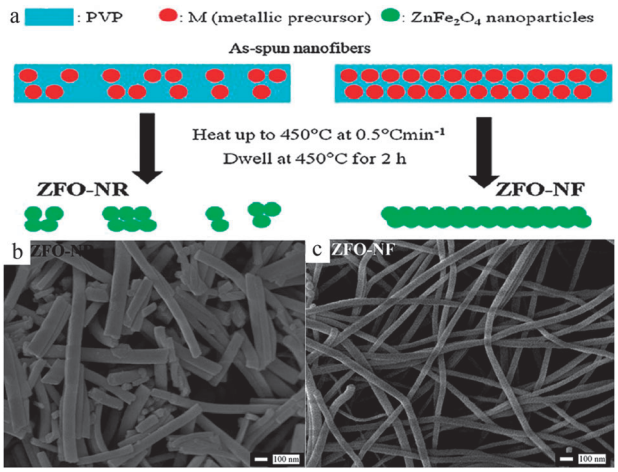

Fig. 3 (a) Formation mechanism of electrospun $ZnFe_2O_4$ nanorods and nanofibers resulting from the high and low viscosities of the solution, respectively. The corresponding FESEM images of the nanorods (b) and nanofibers (c).[86]

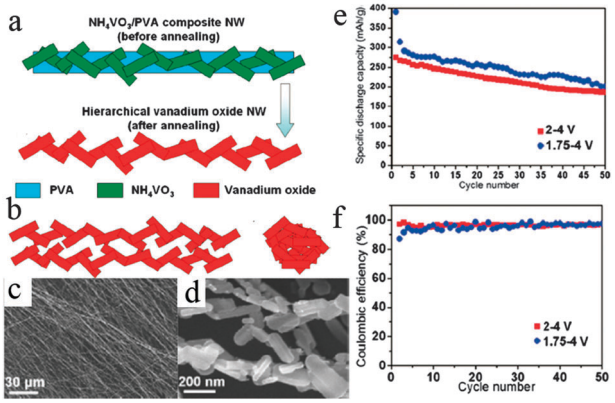

Fig. 4 (a) Schematic illustration of formation of the ultralong hierarchical vanadium oxide nanowires before and after annealing. (b) Side view of two ultralong nanowires near each other and self-aggregation of short nanorods. (c, d) FESEM images of the ultralong hierarchical vanadium oxide nanowires after annealing. (e, f) Cycle performance and Coulombic efficiency of the ultralong nanowires.[90]

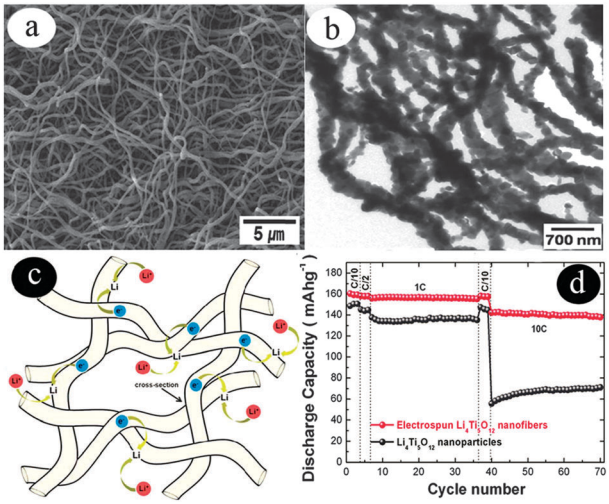

Fig. 5 (a) SEM image and (b) TEM image of the electrospun $Li_4Ti_5O_{12}$ nanofibers. (c) A schematic diagram of the facilitated Li ion and electron transfer in the electrospun $Li_4Ti_5O_{12}$ nanofibers. (d) Capacity retention amounts when conducting charge–discharge cycles at various current rates.[95]

Cheah *et al.*[92] synthesized V_2O_5 nanofibers with the inclusion of various amounts of Al in the V_2O_5 interlayer by a simple electrospinning technique. The moderate incorporation of Al^{3+} could display a higher initial discharge capacity of ~350 mA h g^{-1} and an improved capacity retention of ~85% after 20 cycles at 0.1 C. The higher initial capacity is attributed to the increased space between the VO_5 layers, which enables initial intercalation of a larger amount of Li^+ ions. The improved capacity retention is due to the structural stabilization from the retention of the fibrous morphology during cycling. Interestingly, the inclusion of Al^{3+} in its crystal structure could also result in elevated temperature performance.

Like the electrospun transition metal oxide nanofibers, lithium transition metal oxide (such as $Li_4Ti_5O_{12}$, $LiCoO_2$) nanofibers have also been investigated as electrodes for LIBs. Among these lithium transition metal oxides, $Li_4Ti_5O_{12}$ has been considered as a promising anode material for LIBs because of a higher lithium insertion–deinsertion potential of approximately 1.55 V (*vs.* Li/Li^+), which can avoid the reduction of the electrolyte on the surface of the electrode and the formation of a solid electrolyte interface efficiently. Furthermore, spinel $Li_4Ti_5O_{12}$ shows a very small volume variation during the charge–discharge process, which can result in an excellent cycling stability. However, $Li_4Ti_5O_{12}$ has an inherently low electronic conductivity, which seriously limits its high rate capability.[176–179] To overcome the problem, the use of electrospinning to prepare large surface area 1D $Li_4Ti_5O_{12}$ nanostructures could increase the electrolyte/electrode contact area and provide a shorter path for lithium ion and electron transport, thus resulting in an improved kinetic performance and charge–discharge rate. Jo *et al.*[95] reported tailored $Li_4Ti_5O_{12}$ nanofibers with outstanding kinetics for LIBs (Fig. 5). The electrospun $Li_4Ti_5O_{12}$ nanofibers exhibited a higher capacity compared to $Li_4Ti_5O_{12}$ nanopowders even at high rates exceeding 10 C. This study further highlights the importance of the continuous 1D framework of electrospun nanofibers. On the one hand, the nanofiber structure shows a larger surface area compared to the nanoparticles, which can offer a larger reaction area for Li^+. On the other hand, the 1D structure possesses a smaller diameter, which provides a shorter diffusion length for Li^+ insertion, therefore enhancing the charge transfer and electron conduction along the length direction.

$LiCoO_2$ has been used as a cathode material for commercial rechargeable LIBs due to its high specific energy density (theoretical capacity 140 mA h g^{-1}). However, this electrode material suffers from slow solid state diffusion of the Li^+ cations.[180,181] One of the most investigated strategies to overcome this limitation is to prepare electrospun $LiCoO_2$ nanofibers because of their high specific surface area, short ionic and electronic diffusion pathways and mechanical stability. Interestingly, apart from the nanofibers, the powders derived from electrospun nanofibers possess a higher initial discharge capacity and better cycling stability than those synthesized from regular sol–gel processes.[182] It is self-evident that the electrospun $LiCoO_2$ nanofibers must show a more superior electrochemical performance. Gu *et al.*[96] have demonstrated that $LiCoO_2$ nanofibers showed a higher initial discharge capacity of 182 mA h g^{-1} compared with the conventional powder and film electrodes. Although crystallographic and structural analyses reveal that the $LiCoO_2$ nanofibers allowed more Li^+ insertion and faster solid-state diffusion, greatly increasing the performance of batteries, they still suffered from a large loss of capacity during the charge–discharge process resulting from decomposition reactions, and the phase transition and structural degradation. Similarly, Min *et al.*[97] demonstrated that $Li_{1.2}Ni_{0.17}Co_{0.17}Mn_{0.5}O_2$ nanofibers could provide fast lithium ion intercalation and de-intercalation properties, leading to a higher capacity and enhanced rate capability compared to the co-precipitated particle. However, the capacity retentions were very low due to the poor crystallinity. A promising strategy to solve the problem is to coat these nanofibers with metal oxides or carbon, which will be discussed in the following section.

3.2. Electrospun designed 1D nanomaterials

For electrospun 1D nanomaterials, control of their morphology and structure (such as porous, hollow, core–sheath or hierarchical structure) is of growing interest for lithium storage due to their unique surface properties, which could meet the demand for even higher energy density and performance. Of the proposed candidates, porous or hollow structured 1D nanomaterials have received much attention because these pores can release the volume swell to make the materials more stable and also shorten the Li^+ path length to reduce the overpotential. It is worth mentioning that porous or hollow structured 1D nanomaterials can be easily synthesized by electrospinning and subsequent calcination without involving the multi-step growth of designed shell materials on various removable or sacrificial templates. Herein, the electrospun polymer acted as the template during the formation process of porous or hollow structures. When the electrospun precursor composite nanofibers were calcinated in air, the degradation and oxidation of the polymer and the crystallization of metal oxides occurred simultaneously. The outward diffusion of gaseous species produced by the oxidation of the polymer generated a force to compress the metal oxide nanoparticles in the surface region into a shell. Finally these nanoparticles were mutually connected to generate the porous nanotubes.[101] By this process, various metal oxide nanotubes could be synthesized and applied in LIBs. Among them, NiO[99] and SnO_2[101] have been intensively investigated. Benefiting from their porous and hollow structure, the electrospun porous SnO_2 nanotubes delivered a high initial discharge of 1546 mA h g^{-1} and a discharge capacity of 807 mA h g^{-1} after 50 cycles at a current density of 180 mA g^{-1} from 0 to 2 V, which is substantially higher than the values for previously reported SnO_2 nanostructures, such as SnO_2 nanoparticles, nanotubes, nanowires and hollow nanospheres.[183–187] Also, transition metal oxide spinels (AB_2O_4) with porous tube-like architectures could be prepared by electrospinning. Typically, Luo *et al.*[104] synthesized porous $ZnCo_2O_4$ nanotubes made of interconnected $ZnCo_2O_4$ nanocrystals. The unique structured materials exhibited superior electrochemical lithium-storage performances, including a high reversible capacity (1454 mA h g^{-1} at 100 mA g^{-1}), good cyclability (the specific capacity reaches 1454 mA h g^{-1} after 30 discharge–charge cycles), and an excellent rate performance (the capacity even reaches 794 mA h g^{-1} at a current density as high as 2000 mA g^{-1} after 30 discharge–charge cycles). Different from the solid nanofibers, the formation of porous tube-like architectures is attributed to the Kirkendall effect related to the higher diffusion speed of the melting metal nitrates. Therefore, the subsequent calcination has great effects on the control of the morphology and structure. Wang *et al.*[77] have achieved the controllability and fabricated porous V_2O_5 nanotubes, hierarchical V_2O_5 nanofibers, and single-crystalline V_2O_5 nanobelts by only changing the calcination temperature (Fig. 6). The as-formed V_2O_5 nanostructures exhibited excellent electrochemical performances. In particular, the porous V_2O_5 nanotubes delivered a high power density of 40.2 kW kg^{-1}, whilst the energy density remained as high as 201 W h kg^{-1}.

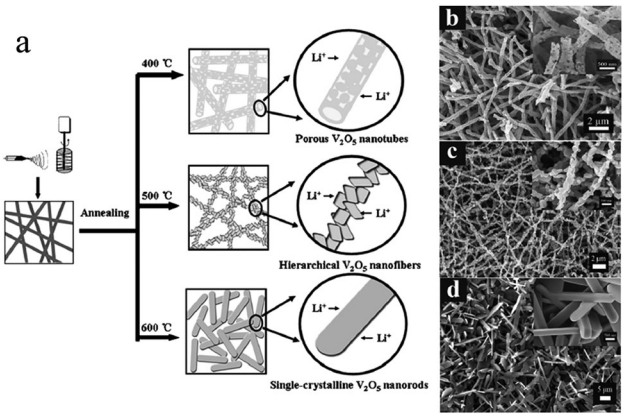

Fig. 6 (a) Preparation of porous V_2O_5 nanotubes, hierarchical V_2O_5 nanofibers, and single-crystalline V_2O_5 nanobelts. The corresponding SEM images are shown in (b)–(d).[77]

Obviously, the electrospun porous nanotubes show fascinating advantages for improving the electrochemical performance of LIBs. On the one hand, the electrospun porous nanotubes inherit the unique properties of the electrospun nanofibers. As mentioned above, the 1D nanofibers exhibit superior electrochemical performances for LIBs compared to their bulk counterparts with micrometer sizes due to the nanoscale effect and the reduced absolute volume change. Moreover, the longer tube-like architecture made up of interconnected nanocrystals greatly limits the mobility of nanocrystals and reduces the agglomeration of nanocrystals during the cycling process. On the other hand, the unique porous tube-like architecture extends the unique properties of the electrospun 1D nanofibers. Obviously, such nanostructures could provide a higher surface area, which could increase the number of accessible sites on the surface of the electrochemically active material and shorten the transport pathway for Li-ion diffusion. Moreover, the central cavity and external pores of the nanotubes not only provide a sufficient space to buffer against the local volume change and mitigate the pulverization problem induced by the volume change during the cycling process, thus leading to an enhanced cyclability, but also promote liquid electrolyte diffusion into the bulk of the electrode as well as providing fast transport channels for the lithium ions, thus leading to an excellent high-rate performance.[101,104]

Further development of electrospun designed 1D nanomaterials is warranted to meet the ever-expanding demand for LIBs. A breakthrough in the electrospinning method was coaxial electrospinning or co-electrospinning, in which a spinneret consisting of two coaxial capillaries is used, with a polymer solution in the shell and either a polymer solution or a non-polymeric Newtonian liquid or even a powder to fill the inner core. Co-electrospinning not only easily produces hollow tubes by the selective removal of the core material (*via* solvents or heat treatment), but also introduces a novel class of core–sheath ceramic or metal structures through the calcination and pyrolysis of metal-containing polymers. In general, mineral oil is used as the inner core material. After calcination, the removal of the oil from the core–sheath fibers results in the formation of hollow fibers. For example,

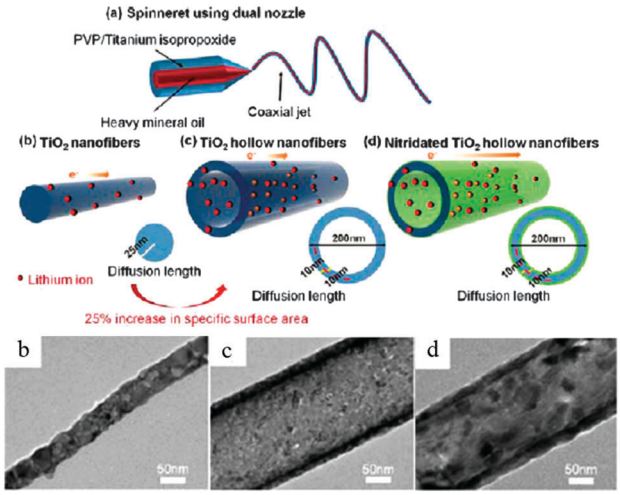

Fig. 7 Schematic illustrations of the coaxial electrospinning spinneret using a dual nozzle (a), TiO_2 nanofibers (b), TiO_2 hollow nanofibers (c), nitridated TiO_2 hollow nanofibers (d), and the corresponding TEM images.[105]

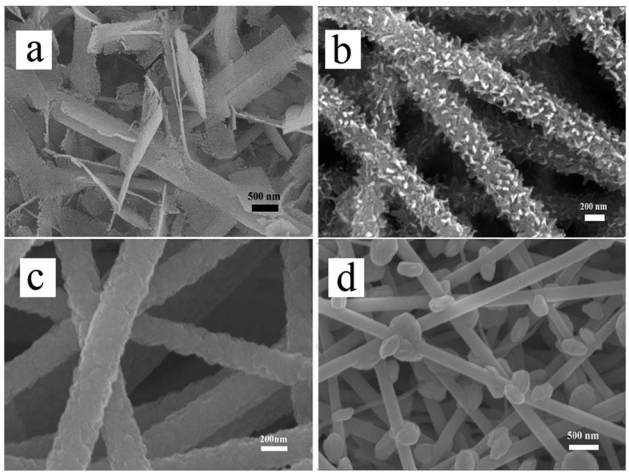

Fig. 8 SEM images of (a) Co_3O_4–TiO_2, (b) Fe_2O_3–TiO_2, (c) Fe_3O_4–TiO_2, and (d) CuO–TiO_2 hierarchical heterostructures.[111]

Han *et al.*[105] have successfully prepared TiO_2 hollow nanofibers by annealing co-electrospun PVP–titanium isopropoxide/mineral oil core–sheath nanofibers (Fig. 7). Interestingly, under an NH_3 atmosphere, thermal treatment could result in the formation of highly conducting TiN/TiO_xN_y layers on the surfaces of the TiO_2 hollow nanofibers. As a result, the nitridated TiO_2 hollow nanofibers exhibited high discharge capacities of about 156 mA h g^{-1}, good capacity retentions of 100% after 100 cycles and a rate capability two times higher compared to that of pristine TiO_2 nanofibers at 5 C. These advantages are mainly attributed to a shorter lithium ion diffusion length and a high electronic conductivity along the surface of the nitridated hollow nanofibers. The replacement of the mineral oil with a polymer solution could obtain metal-containing polymer–polymer coaxial fibers. After calcination, the removal of the polymer from the core–sheath fibers resulted in the formation of metal oxide core–sheath fibers. For example, Gu *et al.*[108] prepared $LiCoO_2$–MgO coaxial fibers by co-electrospinning. Compared to the bare $LiCoO_2$ fibers[96] mentioned above, the coaxial fibers deliver a lower capacity because the presence of the electrochemically inactive MgO coating material can hinder the diffusion of Li^+ cations into/from the $LiCoO_2$ cathode and lower the electronic conductivity of the electrode material,[188] but the cycling performance of the core–shell fibers is greatly increased. After 40 cycles, 90% of the initial discharge capacity of the core–sheath fibers was retained, compared to 52% for the bare $LiCoO_2$ fibers. This is ascribed to the stabilizing effects of MgO, which protects the surface from passive film formation during cycling.[189,190] Therefore, the use of co-electrospun core–sheath coaxial fibers with suitable and optimized substances is a promising strategy to improve the stability and cycling performance.

Surface modification of electrospun 1D nanomaterials is of great significance to improve the electrochemical performance, because such electrode materials may not only promote faster Li^+ diffusion or electron transport but also suppress the particle agglomeration and/or excessive growth. Inspired by this, considerable attempts have been made to build up an integrated smart architecture by combining the electrospinning technique with other synthesis methods, in which the structural features and electroactivities of each component are fully manifested, the interface/chemical distributions are homogeneous at the nanoscale and a fast ion and electron transfer is guaranteed. For example, Luo *et al.*[110] developed a route to synthesize MoO_2-modified TiO_2 nanofibers, comprising a TiO_2 nanofiber core and a thin MoO_2 nanolayer by combining electrospinning and layer-by-layer (LBL) self-assembly processes. They achieved controllability of the thickness of the MoO_2 nanolayer by altering the precursor concentration or the LBL cycles, which could affect the electrochemical properties of the MoO_2-modified TiO_2 nanofibers. Compared to the TiO_2 nanofibers, such electrode materials exhibit a high discharge capacity of 514.5 mA h g^{-1} at 0.2 C over 50 cycles and an excellent rate capability. In addition to combining LBL self-assembly processes, Wang *et al.*[111] combined electrospinning and hydrothermal growth methods to synthesize metal oxide–TiO_2 hierarchical nanofibers. Interestingly, this synthesis strategy can be readily extended to the growth of various metal oxides (*e.g.* Co_3O_4, Fe_2O_3, Fe_3O_4 and CuO) as secondary nanostructures on the primary TiO_2 nanofibers by only altering the precursor parameter (Fig. 8). Compared to the bare TiO_2 nanofibers, the hierarchical nanofibers not only deliver a high reversible capacity of 632.5 mA h g^{-1} and 95.3% capacity retention over 480 cycles, but also show an excellent rate capability. The enhanced electrochemical performance is attributed to the synergetic effect of the two components as well as the unique features of hierarchical heterostructures. Recently, more and more researchers have applied the synergetic effect to design and prepare composite electrode materials, especially electrospun composite materials. They found that enhanced physical and/or chemical properties can be obtained from appropriate surface modifications and the synergetic effect of different building blocks.

3.3. Electrospun 1D composites with CNFs

CNFs prepared *via* electrospinning and following stabilization and carbonization have attracted growing attention in recent years due to their superior mechanical properties and electrical

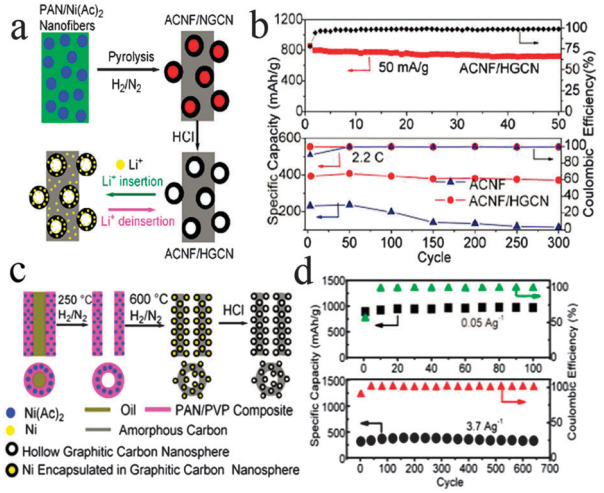

Fig. 9 (a) Schematic diagram illustrating the fabrication procedure and Li^+ insertion and extraction processes inside the ACNF/HGCN electrode. (b) Cycling performance of the ACNF/HGCN and ACNF electrodes at different current rates.[112] (c) Proposed synthesis scheme for ACNHGCNs. (d) Cycling performance of the ACNHGCN electrode at different current densities.[113]

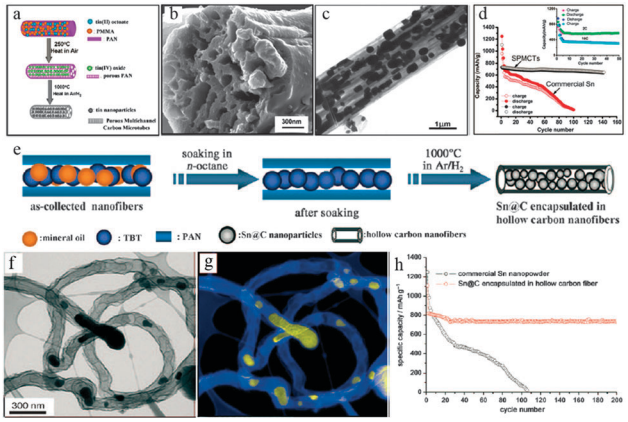

Fig. 10 (a) Proposed synthetic scheme for the SPMCTs. (b) High-magnification cross-sectional image of carbonized PMMA–PAN–tin octoate nanofibers. (c) TEM micrograph of the SPMCTs. (d) Cyclability of the SPMCTs and commercial Sn nanopowder at 0.5 C; the inset displays the discharge capacities of the SPMCTs at 2 and 10 C.[114] (e) Preparation of the SBCNFs. (f) BF zero-loss filtered elastic TEM micrograph of the SBCNFs. (g) Elemental mapping of the nanofibers showing the chemical distribution of carbon (blue) and tin (yellow). (h) Cyclability of the SBCNFs and commercial Sn nanopowder at 0.5 C.[115]

conductivity as well as their unique 1D nanostructures. Although any material with a carbon back-bone can be used as a carbon precursor, the polymer nanofibers which can be converted to CNFs are rather limited (only PAN, PI, PVA, PVDF and pitch). Among these polymers, PAN has received major attention due to its high carbon yield and superior mechanical and electrochemical properties. In particular, CNFs themselves, derived from PAN, can exhibit a high capacity due to their particular microtexture. However, further development for CNFs is necessary to meet the ever-expanding demand for LIBs. In order to obtain CNFs with porous nanostructures, a second component is introduced into the electrospun precursor.[112] After subsequent calcination, acid treatment was used to selectively remove the second component. Using this strategy, the *in situ* formation of hollow graphitic carbon nanospheres in amorphous CNFs (ACNF/HGCN) was reported (Fig. 9a and b). These hollow structures not only provide extra sites for Li^+ storage and sufficient contact between the active material and electrolyte, but also facilitate lithium ion diffusion from different orientations. Moreover, they could serve as buffers for relieving the large volume expansion and shrinkage during cycling. As a result, such electrodes display a high reversible capacity of $\sim$750 mA h g^{-1}, an outstanding rate capability ($\sim$300 mA h g^{-1} at a rate of 8.2 C) and a good cycling stability (a reversible capacity retention of $\sim$100% at 2.2 C after 300 cycles). In addition, coaxial electrospinning is used to prepare carbon materials derived from PAN. Based on this technique, Chen *et al.*[113] prepared amorphous carbon nanotubes decorated with hollow graphitic carbon nanospheres (ACNHGCNs) (Fig. 9c and d). Apart from the unique structures mentioned above,[112] the tube-like architecture further endows this material with a higher reversible specific capacity of $\sim$969 mA h g^{-1}, a more outstanding rate capability ($\sim$330 mA h g^{-1} at a rate of 3.7 A g^{-1}) and a better cycling stability (a capacity retention of $\sim$100% even at 3.7 A g^{-1} after 650 cycles). Obviously, these results show that the hollow graphitic carbon nanospheres as well as the nanopores in the walls of the nanotubes provide more sites for the storage of lithium ions, yielding a much increased specific capacity.

Various metal or oxide nanoparticles have been loaded into CNFs *via* an electrospinning process. For instance, CNFs have been doped with Sn and SnO_2 NPs. It is well known that Sn and SnO_2 have high theoretical capacities, but they suffer from large volume changes and nanoparticle aggregation during cycling. In order to overcome these drawbacks, dispersing nanometric particles into CNFs is feasible because CNFs could act as structural buffers, particle stabilisers, conductive agents and electroactive materials. Yu *et al.*[114,115] have achieved the encapsulation of Sn nanoparticles into porous multichannel carbon microtubes (SPMCTs) (Fig. 10a–c) and bamboo-like hollow CNFs (SBCNFs) (Fig. 10e–g) using a single-nozzle and a coaxial electrospinning technique, respectively. Such porous or hollow carbon shells not only provide appropriate void volume to respond to the large volume change, thus maintaining the stability of the structural arrangements, but also prevent pulverization of the Sn nanoparticles and avoid oxidation of Sn. Moreover, they can also serve as an electron supplier and allow more Li^+ access. As a result, both of them showed good cycling stabilities and excellent rate capabilities (Fig. 10d and h). Specifically, the latter displays a better cycling stability with a reversible capacity of 737 mA h g^{-1} after 200 cycles at 495 mA g^{-1} and a more excellent rate capability (a reversible discharge capacity as high as 480 mA h g^{-1} at 5 C after 100 cycles) (Fig. 10h). In another research article, SnO_2–CNF composites have been synthesized by electrospinning and subsequent thermal treatment.[117] The SnO_2–CNF composites showed a greater discharge capacity than pure carbon nanofibers and displayed a higher initial coulombic efficiency than SnO_2 nanowire. In addition, the achievement of a homogeneous

distribution of SnO_x confined in the CNFs is very desirable for lithium storage,[118] as it can suppress the pulverization and aggregation of the particles and prevent the decomposition of the electrolyte. The strong interaction of the Sn–N bonding between SnO_x and the N-containing CNF matrix could effectively confine the uniformly embedded SnO_x. However, the effect of homogeneous distribution is also limited, because the CNF matrix can only stabilize some Sn from the carbothermal reduction of SnO_2 nanoparticles and the excess Sn melts out of the carbon nanofibers to agglomerate into large crystalline Sn particles, which results in a lower electrochemical performance. To overcome this drawback, light Ni addition can be introduced to locate in the lattice sites of SnO_2 in the form of NiO and prevent SnO_2 from being reduced to Sn and forming large agglomerates.[119]

CNFs have also been loaded with various transition metal oxide nanoparticles such as TiO_2,[120,121] Co_3O_4,[122] MnO_x[123,124] and Fe_xO_y.[125,126] One example is provided by the preparation of TiO_2–CNFs by thermal pyrolysis and oxidization of electrospun titanium(IV) isopropoxide–PAN nanofibers. The composite nanofibers demonstrated an excellent electrochemical performance due to the unique features of encapsulating TiO_2 nanocrystals into a porous carbon matrix.[120] Also, a coaxial electrospinning technique combined with subsequent calcination treatment could be used to develop porous TiO_2–CNFs.[121] The presence of plentiful surface pores enables lithium ions to transport from the outer space into the inner space as storage regions, thus delivering a high specific reversible capacity. In addition, the porous structure and the high conductivity reduce the diffusion paths for Li^+ and facilitate Li^+ access and fast transportation, thus exhibiting a good cycling stability and rate capability. Ongoing research activities have demonstrated that the incorporation of TiO_2 into the CNF matrix could improve the ionic and electronic transport properties of TiO_2 and influence the battery performance. Similarly, electrospun composite nanofibers that interconnect TiO_2 with a conducting additive nanophase (such as carbon nanotubes[191] or graphene[192]) could also improve its Li ion insertion properties. Besides these TiO_2–CNF composite materials, other metal oxide nanoparticles have also been incorporated into the CNF matrix. For example, Zhang *et al.*[122] prepared porous Co_3O_4–CNFs, which show an improved electrochemical performance compared to pure Co_3O_4 nanoparticles. Similarly, carbon-coated MoO_2 nanofibers have also been fabricated.[123] The as-obtained composites reveal a substantial improvement in the electrochemical lithium-storage performance compared to the carbon-free MoO_2 particulates. Studies on metal oxide–CNFs also concern the growth of the secondary nanostructures on the surfaces of the CNFs. Indeed, the direct electrospinning technique limits the loading amount of active materials, which may lower the overall capacity. However, the growth of the secondary nanostructures on the surfaces of the CNFs could increase the loading of the active materials. Recently, electrospun PAN nanofibers have been used as a robust support for the growth of γ-Fe_2O_3 nanoparticles during the hydrothermal process.[125] Such design not only increases the loading of γ-Fe_2O_3 up to more than 60%, but also limits the aggregation of nanoparticles in the following carbonization step, which leads to a high reversible capacity of above 830 mA h g^{-1} after 40 cycles.

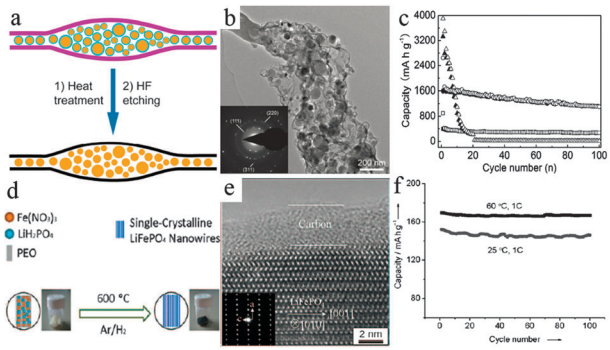

Fig. 11 (a) Schematic illustration, (b) TEM image of the synthetic process for Si@PCNF. (c) Cycling performances of Si@PCNF (circles), CNFs (squares), and Si nanoparticles (triangles).[129] (d) Schematic illustration, (e) corresponding high-resolution TEM image from the marked region and (f) cycling stability of SCNW-LFP at a rate of 1 C at room temperature and at 60 °C.[137]

Many examples have also applied the electrospinning technique to incorporate Si nanoparticles with a higher theoretical capacity (4200 mA h g^{-1}) into the CNF matrix in order to improve its poor cycling performance resulting from large volume changes by up to 400% and nanoparticle aggregation upon the alloying and dealloying reaction with Li^+ ions. Si-loaded CNFs could be prepared by electrospinning PAN–Si nanoparticles.[127,128] Also, the effects of various surrounding confinements of Si nanoparticles have been investigated.[127] Hard confinements resulted in suppressing the volume expansion of Si NPs during the charge–discharge cycles. The electrical conduction of the surrounding material significantly improved the reversible capacity and cycling stability. For example, Zhou *et al.*[129] confined Si nanoparticles in porous CNFs (Si@PCNF) utilizing electrospinning, calcination and subsequent etching (Fig. 11a–c). In their work, the presence of the SiO_x coatings not only favours the homogeneous dispersion of Si@SiO_x nanoparticles in the precursor solution, but also acts as a solid source for hydrogen fluoride etching, thus producing void space between the Si nanoparticles and carbon shell. As a consequence, this material exhibits an improved cycling performance (~1104 mA g h^{-1} at 0.5 A g^{-1} after 100 cycles) as well as excellent rate capabilities (~485 mA g h^{-1} at 10 A g^{-1}). In addition, coaxial electrospinning has also been used to fabricate Si–CNF core–shell fibers with void space in the core section where Si NPs are loaded, which was achieved by choosing Si–PMMA as the core and PAN as the shell.[131] After carbonization, PAN can still remain stable in the shell. By contrast, PMMA could be evaporated at relatively low temperatures, which results in the formation of void space in the core of the fibers. This unique structure indeed shows a high capacity of 1384 mA h g^{-1} at a rate of C/10 and an outstanding cycle life of 300 cycles with 99% capacity retention. In particular, it is noteworthy that such electrode materials can retain 52.2% of the original capacity even when the current increases 80 times (from C/10 to 12 C). Obviously, it is critical for decent cell operation that void space is formed in the core section where the Si NPs are loaded because the void space can accommodate the volume expansion of Si. Another promising

strategy to improve the performance of Si is adding other components (such as graphitized carbon[132] or TiO_2[133]) into the electrospun Si–CNF composite.

Lithium metal oxides could also be loaded into CNFs *via* electrospinning. For example, $Li_4Ti_5O_{12}$-loaded CNFs could be prepared by electrospinning either PAN–tetrabutyltitanate–lithium acetate[134] or PAN–$Li_4Ti_5O_{12}$ nanoparticles.[135] During the calcination process, the pyrolysis of PAN and the conglutinated $Li_4Ti_5O_{12}$–CNFs could result in the formation of nanopores, mesopores, three-dimensional nanoweb architectures, and a large surface-to-volume ratio, which greatly improve the lithium storage properties due to enlarging the electrode–electrolyte contact area and shortening the lithium ion diffusion pathways during the charge–discharge processes.[134] Moreover, the incorporation of $Li_4Ti_5O_{12}$ into CNFs could effectively avoid the formation of large aggregates of $Li_4Ti_5O_{12}$ nanoparticles, thus improving the reversible capacities.[135] In addition, electrospun $LiFePO_4$-loaded carbon materials have also been obtained.[136,137] In particular, highly electroactive carbon-coated single-crystalline $LiFePO_4$ nanowires (SCNW-LFP) have been produced by electrospinning (Fig. 11d–f).[137] It is noteworthy that electrospun polycrystalline nanomaterials can be easily prepared, but electrospun single-crystalline nanomaterials are quite rare. With the help of the single-crystalline $LiFePO_4$ nanowires and the protective carbon coating, the electrode materials not only delivered a higher capacity and a better rate performance than the commercial carbon-coated $LiFePO_4$ particles, but also exhibited a good cycling performance at different temperatures. Obviously, the single-crystalline nanomaterials play a very important role in improving the battery performance. Certainly, the affect of protective carbon can not be ignored. For example, the incorporation of some other electroactive carbon materials, such as graphene,[193] carbon nanotubes,[194] *etc.*, can also improve the electrochemical performance.

3.4. Electrospun flexible electrodes with CNFs

Traditionally, the electrodes in LIBs are prepared using a slurry-casting method by mixing active materials with polymer binders (such as PVDF) and conductive agents (such as carbon black), and then casting the mixtures on Cu (negative electrode) and Al (positive electrode). However, the presence of binders, which are insulating and electrochemically inactive, not only reduces the overall volumetric/gravimetric energy density by adding weight to the electrodes, but also influences the cycling stability due to the side effects between the electrolyte and these inactive materials. In addition, the heavy weight of the metal current collectors also has a detrimental effect on the gravimetric capacity of the whole battery system. Thus, the preparation of flexible, binder-free (no need for polymer binders) and free-standing (no need for metal substrates as current collectors) electrodes simplifies the electrode preparation process, greatly reduces the inactive weight and cost of the cells, and significantly improves the electrochemical performance of LIBs.[195,196]

Electrospinning is the most attractive method for fabricating CNF-based composite flexible electrodes, which can be directly used as electrode materials without any conductive agent, binder or current collectors, because the electrospun CNFs can form highly porous free-standing flexible mats, thus largely simplifying the fabrication process. Therefore, the search for electrospun flexible electrode materials with improved LIB performances is growing vigorously. Earlier work focused on attaching various electrospun flexible materials onto metal substrates (copper foil or nickel meshes) to be used as the working electrode without adding any binder or conductive agents. Typically, Zhang and coworkers have reported a series of papers about different electrospun flexible electrode materials with CNFs. In their work, the electrospun porous flexible CNFs could be fabricated simply by either annealing the electrospun bicomponent polymer[138,139] or etching the carbon–inorganic composite nanofibers.[140,141] Also, transition metal-loaded CNFs have been fabricated due to their good electrical conductivities.[142,143] Metal oxides,[144–148] Si[149–151] and $LiFePO_4$[152,153] have also been loaded into free-standing and flexible CNF films. In addition, Wu *et al.*[154] engineered an empty space between Si nanoparticles by encapsulating them in hollow carbon tube mats and then laminating this freestanding film on copper foil to be directly used as the working electrode. As mentioned above, the thin carbon layers enhanced the electrical conductivity of the electrode. Introducing ample empty space inside the hollow tubes could circumvent the huge volume changes and aggregation of silicon during electrochemical cycling, thereby resulting in further improved performances. Also, this design effectively prevented unstable solid–electrolyte interphase (SEI) formation.[154] Better still, each carbon tube was directly connected to the current collector and acted as a fast and stable electron transfer channel, enabling a stable cycling of the entire electrode as well as high charge and discharge rates. As a result, the electrode demonstrated a high gravimetric capacity of $\sim$1000 mA h g^{-1} at 1 A g^{-1} and a long cycle life of 200 cycles with 90% capacity retention. In addition to attaching electrospun flexible materials onto copper foil, they could be also attached onto nickel meshes to be directly used as the working electrode without adding any binder or conductive agents.[155–157]

Electrospun flexible electrode materials could be directly used as the working electrode without current collectors or any additives, which will further simplify the cell packing process, resulting in further improvements in both the energy density and power density for LIBs. For example, Wang *et al.*[158] fabricated lignin-derived fused electrospun carbon fibrous mats and directly used them as the working electrode (Fig. 12). Interestingly, they found that the N-doped carbon fibrous mats could be prepared *via* electrospinning followed by carbonization and thermal annealing with urea, and demonstrated that the performance of the obtained electrode materials could be further improved by incorporating heteroatoms. As a result, the charge capacity of the free-standing electrode was further improved to as high as 576 mA h g^{-1} and it still maintained a good capacity of $\sim$200 mA h g^{-1} even at a high current rate of 2000 mA g^{-1}.

Also, metals,[159,160] metal oxides[161–165] or metal sulfides[166] can be encapsulated in flexible electrospun CNFs as free-standing working electrodes. In particular, Ge nanoparticles have been introduced into flexible electrospun CNFs. Compared to the Si

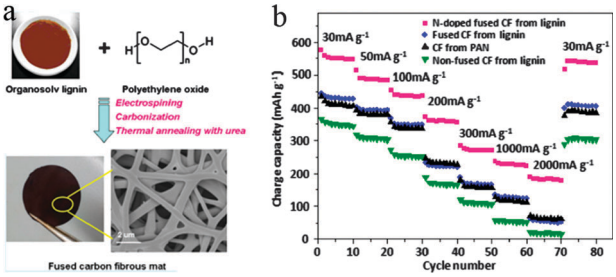

Fig. 12 (a) Schematic illustration of the synthesis process for the free-standing and flexible fused carbon fibrous mats. (b) Charge capacities of the carbon samples at different current rates.[158]

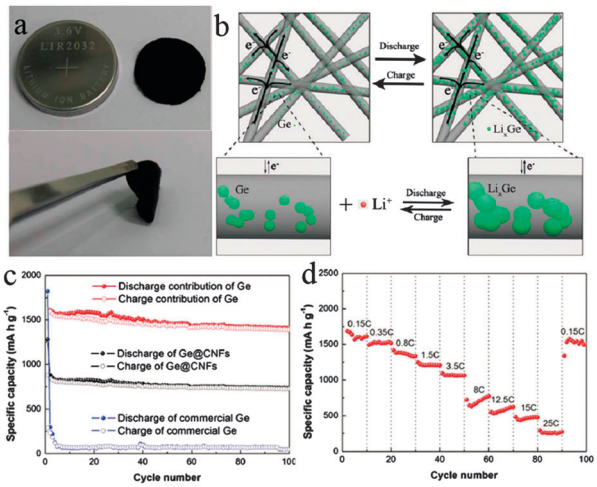

Fig. 13 (a) Photographs of the free-standing and flexible Ge@CNF electrodes. (b) Schematic illustration of the alloying/de-alloying reaction mechanism of Ge@CNFs during cycling. (c) Capacity–cycle number curves of the Ge–CNF and commercial Ge powder electrodes at 0.15 C. (d) Discharge capacity of the Ge–CNF electrode as a function of discharge rate.[160]

anode, although Ge shows a lower theoretical capacity (1624 mA h g^{-1}), it possesses an excellent lithium-ion diffusion coefficient (400 times higher than Si). Therefore, Ge anodes for LIBs have also received much attention. However, the practical application of Ge anodes is also subjected to the poor cyclability resulting from the drastic volume changes and nanoparticle aggregates during cycling. To minimize the volume strain and enhance the cycling stability, encapsulation of Ge nanoparticles into electrospun flexible carbon nanofibers (Ge@CNFs) has been reported to be promising (Fig. 13).[160] Further, this type of composite could be used as a free-standing anode, which exhibited an excellent electrochemical performance with a reversible specific capacity of 1420 mA h g^{-1} after 100 cycles at 0.15 C (only 0.1% decay per cycle). Even at a high current of 1 C, the free-standing electrode still delivered a reversible specific capacity of 829 mA h g^{-1} after 250 cycles. Obviously, the free-standing electrode as well as the synergistic effects of Ge nanoparticles, CNFs, and the interconnected CNF network could effectively accommodate the huge volume change and aggregates of Ge nanoparticles. In addition, Zhang *et al.*[163] synthesized electrospun CNFs containing ultrafine SnO_x particles (SnO_x–CNF) and

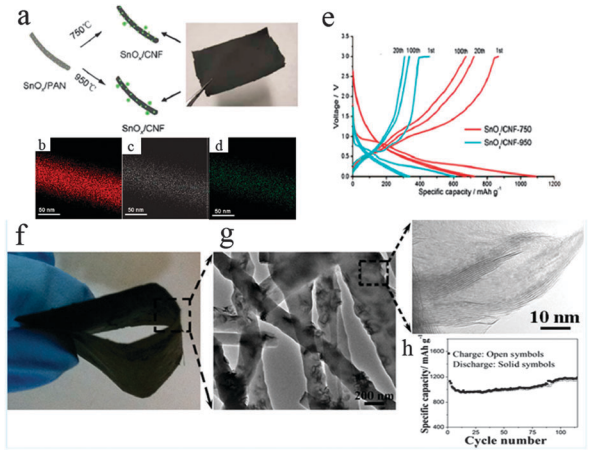

Fig. 14 (a) Illustration of the SnO_x–CNF fabrication process. (b)–(d) Elemental mapping of carbon, tin, and oxygen, respectively. (e) Charge–discharge curves of the SnO_x–CNF composites obtained at the 1st, 20th, 100th cycles at 0.5 A g^{-1}.[163] (f) Photograph and (g) SEM images of the free-standing and flexible MoS_2/C nanofibrous mats. (h) Cycling performance of the MoS_2/C nanofibrous mats at 50 mA g^{-1}.[166]

used them as a free-standing working electrode, which delivered a remarkable capacity of 674 mA h g^{-1} after 100 cycles at 0.5 A g^{-1} (Fig. 14a–e). The good electrochemical performance is attributed to the uniform embedding of the ultrafine and amorphous SnO_x particles on the atomic scale in the conductive CNFs, which makes the electrochemical reaction highly reversible. Most recently, Zhao *et al.*[166] encapsulated disordered thin MoS_2 nanoflakes in amorphous CNFs to fabricate highly flexible MoS_2/C nanofibrous mats (Fig. 14f, g). This free-standing working electrode showed a high capacity of ~1200 mA h g^{-1}, and a long cycling performance of 1150 mA h g^{-1} after 100 cycles. Apart from the advantages of good electron transport provided by the high aspect ratio of the electrospun CNFs and the effective confinement of the active material by the carbon matrix, the choice of MoS_2 with a higher capacity and layered structure is also important. On the one hand, the dispersion of thin and flexible MoS_2 nanosheets in the CNFs gives the composite excellent flexibility. On the other hand, the fine thickness and multilayered structure of the MoS_2 sheets with an expanded interlayer spacing exhibits a higher Li^+ ion capacity. In addition, the incorporation of $LiFe_{1-y}Mn_yPO_4$ into the flexible electrospun CNFs as a self-supporting cathode has also showed an improved performance, especially in terms of the cycling stability and rate performance.[167]

4. Electrospun nanomaterials in sodium-ion batteries

Sodium-ion batteries (SIBs) are attracting considerable renewed interest as promising candidates for new battery systems, especially for large-scale and long-term electric energy storage applications, due to their cost advantages (6th most abundant element in the Earth's crust). Because of the relatively heavier weight, the larger radius (0.102 nm) and the lower-reducing

potential of Na, the gravimetric and volumetric densities of a SIB do not exceed those of its Li analogue.[197–208] Given the field of large-scale electric energy storage, energy density is not a critical issue. Thus, developing room-temperature "rocking-chair" SIBs with a similar working principle as LIBs for large-scale electric energy storage is still a reasonable alternative.[209–214] However, compared to years of research about electrospun lithium insertion materials, there has been relatively limited research about electrospun materials for SIBs.[215–223] So far, research has mainly focused on the electrode materials based on electrospun 1D composites with CNFs. Similarly, along with the avenues of research about electrospun flexible electrodes for LIBs, electrospun flexible electrodes for SIBs are a rapidly growing and enormously promising field. As a timely overview, recent studies on electrospun SIB electrode materials are highlighted in this section.

4.1. Electrospun 1D composites with CNFs

It has been well established that graphite, which is the dominant anode material in today's commercial LIBs, has a very low sodium intercalation capacity of 32–35 mA h g^{-1} because sodium hardly forms staged intercalation compounds with graphite.[224,225] Therefore, non-graphitic carbon materials are now considered the most suitable and dominant candidate materials. So far, various carbonaceous materials, such as coke,[226,227] carbon black,[228] pyrolytic carbon,[229] carbon fiber,[230] template carbon,[231] hollow carbon nanowires,[202] hollow carbon nanospheres,[20] and nitrogen-doped porous carbon nanosheets[21] have been studied because of their large interlayer distance and disordered structure. Generally, good Na-ion insertion properties need a short diffusion distance, a disordered structure and a large interlayer distance between the graphitic sheets. As mentioned above, electrospun CNFs possess these characteristics, which appear to be the most suitable anode materials for SIBs. Very recently, Chen *et al.*[215] fabricated electrospun CNFs and for the first time used them as anode materials for SIBs. Due to their weakly ordered turbostratic structure and a large interlayer spacing between the graphene sheets, the electrospun CNFs showed a good electrochemical performance, including high reversible capacities of 233 and 82 mA h g^{-1} at 0.05 A g^{-1} and 2 A g^{-1}, respectively, and a good cycling stability of 97.7% capacity retention ratio over 200 cycles.

As for the development progress of LIBs, the capacity of anode materials for SIBs still needs to be improved to meet the rigorous requirements for practical applications. Recently, various metals and their alloys, such as Sn,[210,232,233] Sb,[234,235] Ge,[236] and SnSb alloys,[237,238] have attracted considerable interest due to their appropriate sodium inserting potential and high theoretical specific capacities. However, severe structural degradation resulting from large volume expansion and contraction during electrochemical cycling also severely hinders their application in SIBs. To solve this problem, researchers have attempted to develop composites of nanostructured particles supported by carbon matrices. Interestingly, it is easy and effective to achieve such structures for electrospinning as mentioned above, which will promote electrospinning to be used extensively to prepare the electrode materials for SIBs, thus making good

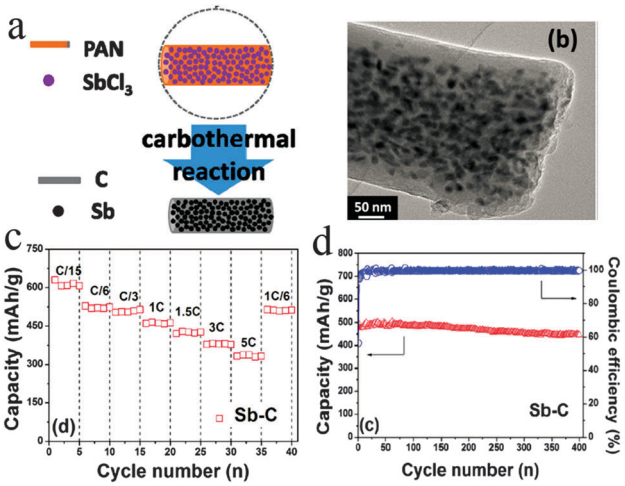

Fig. 15 (a) Schematic illustration of the preparation process for the Sb–C nanofibers. (b) TEM image of the Sb–C nanofibers. (c) Rate capability of the Sb–C electrode at various current rates. (d) Cycling performance of the Sb–C electrode at C/3.[216]

progress on SIB development. For example, Wu *et al.*[216] embedded Sb nanoparticles in CNFs to form Sb–C composite nanofibers through electrospinning and subsequent calcination (Fig. 15). They confirmed that the Sb nanoparticles were embedded homogeneously in the uniform CNF matrix, which not only prevents the aggregation of the Sb nanoparticles, but also provides a conductive and buffering matrix for the effective release of mechanical stress resulting from Na-ion intercalation and deintercalation. As a result, cycled between 0.01 V and 2.0 V, the Sb–C nanofibers delivered a high reversible capacity of 631 mA h g^{-1} at C/15 (40 mA g^{-1}), a good cycling stability of 90% capacity retention after 400 cycles and an improved rate capability of 337 mA h g^{-1} at 5 C. In addition, porous SnSb–C composite nanofibers prepared by encapsulating the highly dispersed and small SnSb nanoparticles into porous CNFs also showed an enhanced electrochemical performance.[217] It is obvious that achieving a homogeneous dispersion of doped materials in the CNF matrix gives the composite electrode materials an improved electrochemical performance. Although constructing electrospun 1D composites is beneficial to improving the SIB performance, we must not neglect the fact that the fluoroethylene carbonate (FEC) additive plays a critical role in manipulating the solid electrolyte interphase (SEI) formation. It is well known that the SEI formation resulting from side reactions between the electrolyte and the electrode and the decomposition of the electrolyte can significantly influence the LIB performance. Considering the high chemical reactivity of Na, the electrolyte decomposition and the SEI formation must be more serious and critical for SIBs. Therefore, it is necessary to add the FEC additive because its presence could modify the passivation layer of the electrode surface, suppress the side reactions of the electrolyte and minimize the decomposition of the electrolyte.[239–243] As a result, a thin, chemically/mechanically stable and structurally compact SEI film is formed, which could significantly improve the cycling stability and rate capability.

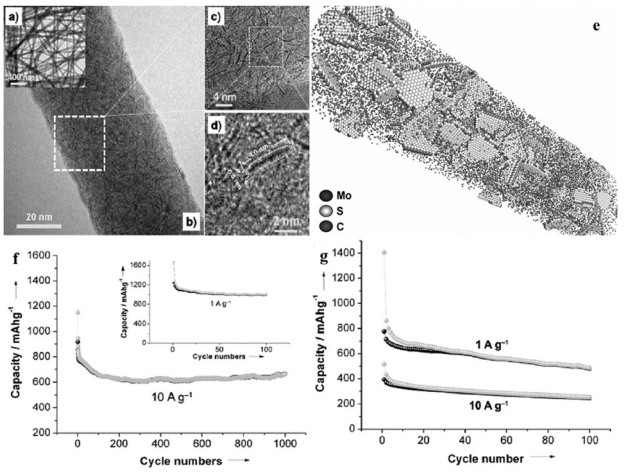

Fig. 16 (a) TEM-BF micrograph. (b)–(d) HRTEM images of the ultrathin MoS_2 embedded in the carbon nanofiber. (e) Schematic representation based on TEM modeling studies to demonstrate the unique morphology of such a composite: single layered ultrasmall MoS_2 nameplates embedded in a thin carbon nanofiber. Cycling performances of LIBs (f) and SIBs (g).[218]

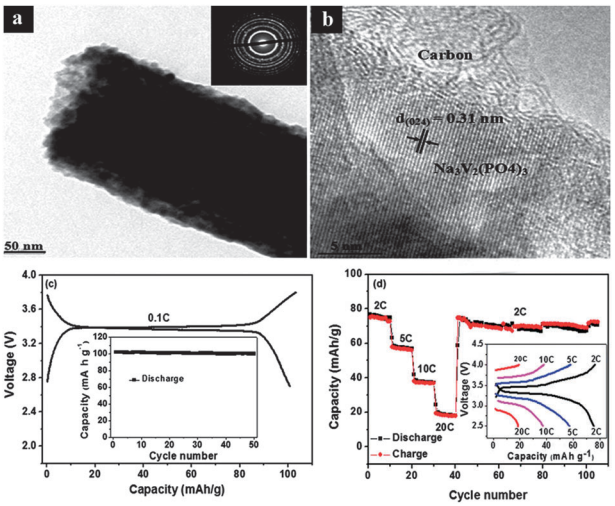

Fig. 17 TEM (a) and HRTEM (b) images of the $Na_3V_2(PO_4)_3$/C nanofiber, the inset shows the SAED pattern of a single nanofiber, which indicates that these $Na_3V_2(PO_4)_3$ composite fibers are polycrystalline and well-crystallized. (c) The first voltage–capacity curves at a rate of 0.1 C, and the inset shows the cycling stability of the $Na_3V_2(PO_4)_3$/C nanofiber at 0.1 C. (d) Cycling performance of the $Na_3V_2(PO_4)_3$/C cathode at different current densities.[220]

Also, a variety of metal sulfides, such as Sb_2S_3,[244] MoS_2,[245] NiS,[246] and SnS_2,[247] have attracted considerable interest for SIBs. MoS_2 is the most attractive layered materials as it exhibits high theoretical specific capacities. However, MoS_2-based electrode materials also suffer from rapid capacity fading and low conductivities. In this respect, combining carbon with the poorly conductive metal sulfides was confirmed to be an effective way to enhance electron and mass transport. Very recently, Zhu *et al.*[218] embedded MoS_2 nanoplates in CNFs by electrospinning (Fig. 16). Interestingly, these nanofibers were very thin, with a diameter of only ~50 nm. Moreover, the embedded MoS_2 nanoplates were extremely thin and small, with a thickness of only 0.4 nm and a lateral dimension of 4 nm. These unique nanostructures as well as the single-layered nature by spatial isolation and the lateral confinement in the carbon matrix not only minimize transport problems in the sulfide in all directions, but also render the conversion reversible. As a result, this electrode material exhibited a high capacity and remarkable cycling performance for both lithium storage (the capacity is 661 mA h g^{-1} even after 1000 cycles at a high current density of 10 A g^{-1}) and sodium storage (the capacity is 484 and 253 mA h g^{-1} after 100 cycles at 1 and 10 A g^{-1}, respectively). The lower capacity for sodium storage compared to lithium storage results from the difference in the thermodynamics and kinetics for insertion of Li^+ and Na^+ ions. Even so, the excellent cycling stability for sodium storage without adding the FEC additive highlights the importance of the unique structure of the composite for SIBs.

In addition to the electrospun metals, their alloys or metal sulfide materials, lithium–sodium metal oxides could also be incorporated into electrospun carbon materials. In the same group, tiny $Li_4Ti_5O_{12}$[219] and $Na_3V_2(PO_4)_3$[220] nanoparticles were embedded in electrospun CNFs. In particular, NASICON-type $Na_3V_2(PO_4)_3$ has recently been investigated as a promising cathode material for SIBs. However, considering the poor electronic conductivity of phosphates, uniformly dispersing $Na_3V_2(PO_4)_3$ with the reducing particle sizes into the electrospun electrically conductive carbon matrix is still a major strategy to improve the electronic conductivity (Fig. 17). Moreover, such structures also minimize the stain problems and improve the transport path. As a result, at a rate of 0.1 C, the $Na_3V_2(PO_4)_3$/C cathode showed a high initial charge and discharge capacity of 103 and 101 mA h g^{-1}, respectively, and retained stable discharge capacities at high current densities.

4.2. Electrospun flexible electrodes with CNFs

As mentioned above, the preparation of flexible, binder-free (no need for polymer binders) and free-standing (no need for metal substrates as current collectors) electrodes not only simplifies the electrode preparation process and reduces the inactive weight and cost of the cells, but also significantly improves the electrochemical performance of LIBs. In view of these advantages, applying electrospun flexible free-standing electrodes in SIBs will attract more and more attention. It is especially necessary to further improve both the volumetric energy and power density for SIBs. Fortunately, the intensive development of LIBs has paved the way for further improvements in SIBs, and some attempts have been made to verify its feasibility. For example, Li *et al.*[222] prepared a lightweight and flexible free-standing porous CNF (P-CNF) electrode by pyrolysis of PAN/Pluronic F127 nanofibers (Fig. 18). In their work, triblock copolymer Pluronic F127 was chosen as a soft template to create CNFs with plenty of micropores, which are beneficial for sodium ion storage. In addition, hierarchical porous channels resulting from the interpenetrating P-CNF films effectively shortened the transport length for both sodium ions and electrons. As a result, the obtained P-CNFs deliver a good reversible capacity of

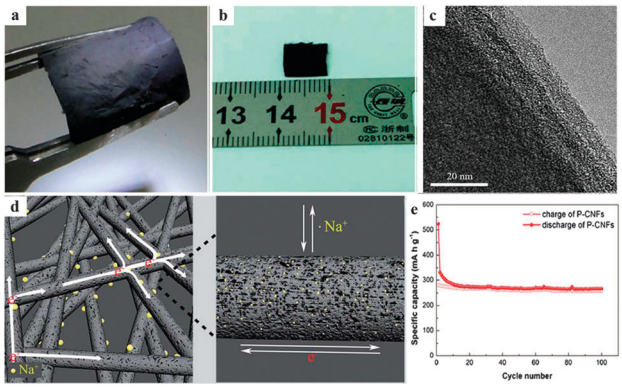

Fig. 18 (a) and (b) Photographs of the free-standing and flexible P-CNF electrode. (c) HRTEM image of the P-CNF. (d) Schematic illustration of the sodium storage mechanism in P-CNFs. (e) Cycling performance of the P-CNF electrode at 50 mA g^{-1}.[222]

266 mA h g^{-1} after 100 cycles at 50 mA g^{-1} and an enhanced rate capability of ~60 mA h g^{-1} at a high rate of 500 mA g^{-1}. Therefore, developing flexible electrodes for SIBs is feasible and necessary to improve the electrode performance.

As well as the electrospun flexible CNF electrode discussed above, flexible electrodes made from CNFs embedded with metals have also been prepared with improved electrochemical performances. For example, Zhu *et al.*[223] prepared a binder-free and current collector-free flexible Sb/C electrode by electrospinning and subsequent calcination (Fig. 19). In their work, tiny Sb nanoparticles with a diameter of ~30 nm were uniformly encapsulated into interconnecting CNFs (denoted as SbNP@C). This unique nanostructure integrates two virtues: (1) Sb nanoparticles were well dispersed and confined into the conductive CNF matrix, which can effectively tolerate the massive volume changes, prevent pulverization, and preserve electrode integrity during the Na alloying/dealloying reaction; (2) the CNFs themselves serve as a current collector, which avoids a loss of contact between the active materials and current collector/conductive additives resulting from the huge volume change for the regular electrode with a metal current collector, binder, and conductive additives. As a consequence, the SbNP@C electrode showed a

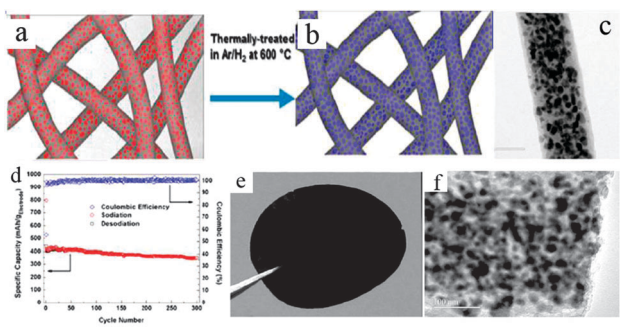

Fig. 19 (a) and (b) Schematic illustration of the synthesis process for the SbNP@C electrode. (c) TEM image of the carbon-encapsulated Sb fibers. (d) Cycling performance of the SbNP@C electrode at 0.1 A g^{-1}. (e) Digital image of the SbNP@C electrode after 300 charge discharge cycles. (f) TEM image of the after-cycled fibers in the SbNP@C electrode.[223]

high initial capacity of 422 mA h g^{-1} and retained 350 mA h g^{-1} after 300 cycles at 100 mA g^{-1}.

Obviously, compared to the great surge in developing electrospun materials for LIBs, there has been relatively limited research about electrospun materials for SIBs. Therefore, future efforts should focus on the preparation of electrospun materials for SIBs, especially binder-free and current collector-free flexible electrodes. In spite of this, the rapid development of this field is very encouraging and electrospun flexible electrodes with high performance provide promising alternatives to build flexible SIBs.

5. Summary and perspective

In this review, we have summarized almost all the progress in electrospun electrode materials for LIBs, covering the structure evolution from solid nanofibers into designed 1D nanomaterials, then 1D composites with CNFs, and finally into flexible electrode materials with CNFs. The breakthrough of synthetic methodologies is likely to provide opportunities to meet some of the challenges associated with the critical physico-chemical and electrochemical parameters of LIBs because the structural control of nanomaterials can be as important as the composition of the materials themselves. In addition, recent studies on electrospun SIB electrode materials have been timely presented. Along with the avenues of research about electrospun electrode materials for LIBs, more attention has been paid to electrospun SIB electrode materials. By constructing controllable 1D nanostructures, one can take full advantage of the electrospun materials, such as shorter diffusion pathways, faster Li intercalation kinetics, good mechanical strengths, high surface areas and porosities, mitigated charge transfer resistance and enhance ionic conductivities. Thus, the outstanding electrochemical performance of electrospun electrode materials will stimulate their wide use in commercial LIBs or SIBs, and even in flexible, lightweight, stretchable, foldable battery devices. Despite the considerable achievements made so far, there exists substantial room for the development of high performance battery materials and the increasing interest in electrospun materials will provide great opportunities for advanced battery systems in the years ahead.

1. Design with more controllability. In view of the above-mentioned discussion, the structural and morphological control of nanomaterials is of great importance. Although a large number of controllable 1D electrode materials have been reported, when designing more beneficial structures to meet the market demands for high-performance LIBs or SIBs the following factors must be considered: (1) to develop uniform nanofibers with diameters below 50 nm. Thin 1D materials could provide shorter diffusion pathways and faster Li intercalation kinetics; (2) to obtain uniaxially aligned nanofibers. Electrospinning with improved designs or additional set ups[248–250] could produce aligned nanofibers that can be more useful in energy conversion devices due to the unique physicochemical properties provided by their anisotropy and high surface-to-volume ratio; (3) to prepare micro/nano structured composite nanofibers. Multinozzle electrospinning could achieve controllable

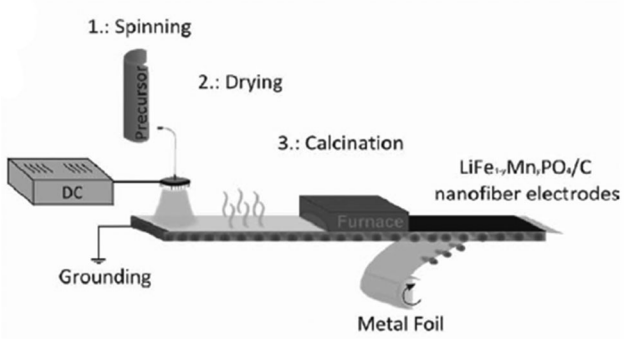

Fig. 20 Cartoon showing the preparation method of the nanofiber electrodes. The process could be used on an industrial scale and the sequence was spinning, drying and calcining.[167]

composite fibers with different sizes and morphologies,[251,252] thus taking advantage of the synergistic effect of diverse properties; (4) to electrospin conjugated or conductive polymers. Such 1D materials could not only show the toughness structure of the polymers to buffer the huge volume change during the charge–discharge cycling, especially for the larger Na^+ ion, but also avoid further heat treatment at high temperatures in the formation process of CNFs; (5) to incorporate heteroatoms into 1D nanofibers. The presence of heteroatoms at the carbon surface can enhance the reactivity and electric conductivity, and hence improve the Li^+/Na^+-ion storage capacity.[253–256]

2. To realize large scale production. The synthesis of self-supported nanofiber electrodes consists of electrospinning nanofiber films (1 – Fig. 20), followed by a drying step (2 – Fig. 20), calcination (3 – Fig. 20) and casting of the current collector. Since these procedures are scalable methods, the electrode production is shown exemplarily as a continuous process (Fig. 20).[167] However, current electrospinning processes commonly have relatively low production rates (from the perspective of industrial manufacture) and involve toxic and corrosive organic solvents in the preparation of the precursor solutions. In the near future, it is likely that research effort will be focused on engineering an environmentally friendly electrospinning process with a faster rate.

3. Developing all electrospun flexible batteries. In addition to electrospun flexible cathode and anode materials, electrospinning is quite a suitable technique for the development of highly porous and thick separators with high electrolyte intake, good homogeneity and ionic conductivity. Traditionally, chemically and mechanically stable micro-porous polymer membranes suffer from a low thermal stability, wettability and porosity, which affect the overall battery performance. Alternatively, electrospun nanoporous polymers have a high porosity and an interconnected open pore structure, which can contribute to a high ionic conductivity and sufficient mechanical strength. Thus, they may be more suitable for battery fabrication.

4. The search for advanced battery systems. In recent years, electrospun 1D materials have been widely used in many energy conversion and storage devices, such as fuel cells, dye-sensitized solar cells, LIBs and supercapacitors, which will pave the way for advanced battery systems, such as lithium–sulfur, sodium-ion and lithium–air batteries. With joint endeavors from all parties concerned, we believe that high performance electrospun 1D materials can be applied in commercialized high-performance advanced battery systems in the near future.

Acknowledgements

This work was supported in part by the National Natural Science Foundation of China (51471075, 51401084 and 51101070), and Jilin University Fundamental Research Funds.

Notes and references

1 M. Winter and J. B. Brodd, *Chem. Rev.*, 2004, **104**, 4245–4270.
2 J. M. Tarascon and M. Armand, *Nature*, 2001, **414**, 359–367.
3 P. Poizot, S. Laruelle, S. Grugeon, L. Dupont and J. M. Tarascon, *Nature*, 2000, **407**, 496–499.
4 R. Berthelot, D. Carlier and C. Delmas, *Nat. Mater.*, 2011, **10**, 74–80.
5 N. Yabuuchi, M. Kajiyama, J. Iwatate, H. Nishikawa, S. Hitomi, R. Okuyama, R. Usui, Y. Yamada and S. Komaba, *Nat. Mater.*, 2012, **11**, 512–517.
6 J. B. Goodenough, H. D. Abruña and M. V. Buchanan, *Basic Research Needs for Electric Energy Storage: Report of the Basic Energy Sciences Workshop on Electrical Energy Storage*, U.S. Department of Energy, Office of Basic Energy Sciences, Washington, DC, 2007.
7 Y. Wang and G. Z. Cao, *Adv. Mater.*, 2008, **20**, 2251–2269.
8 S.-W. Kim, D.-H. Seo, X. H. Ma, G. Ceder and K. Kang, *Adv. Energy Mater.*, 2012, **2**, 710–721.
9 M. D. Slater, D. Kim, E. Lee and C. S. Johnson, *Adv. Funct. Mater.*, 2013, **23**, 947–958.
10 V. L. Chevrier and G. Ceder, *J. Electrochem. Soc.*, 2011, **158**, A1011–A1014.
11 V. Palomares, P. Serras, I. Villaluenga, K. B. Hueso, J. Carretero-González and T. Rojo, *Energy Environ. Sci.*, 2012, **5**, 5884–5901.
12 J. B. Goodenough, *Acc. Chem. Res.*, 2013, **46**, 1053–1061.
13 H. L. Pan, Y.-S. Hu and L. Q. Chen, *Energy Environ. Sci.*, 2013, **6**, 2338–2360.
14 J. F. Qian, M. Zhou, Y. L. Cao, X. P. Ai and H. X. Yang, *Adv. Energy Mater.*, 2012, **2**, 410–414.
15 Y. L. Cao, L. F. Xiao, W. Wang, D. Choi, Z. M. Nie, J. G. Yu, L. V. Saraf, Z. G. Yang and J. Liu, *Adv. Mater.*, 2011, **23**, 3155–3160.
16 Z. L. Jian, W. Z. Han, X. Lu, H. X. Yang, Y.-S. Hu, J. Zhou, Z. B. Zhou, J. Q. Li, W. Chen, D. F. Chen and L. Q. Chen, *Adv. Energy Mater.*, 2013, **3**, 156–160.
17 Y. Sun, L. Zhao, H. Pan, X. Lu, L. Gu, Y.-S. Hu, H. Li, M. Armand, Y. Ikuhara, L. Chen and X. Huang, *Nat. Commun.*, 2013, **4**, 870.
18 Z. L. Jian, L. Zhao, H. L. Pan, Y.-S. Hu, H. Li, W. Chen and L. Q. Chen, *Electrochem. Commun.*, 2012, **14**, 86–89.

19 L. Wang, Y. H. Lu, J. Liu, M. W. Xu, J. G. Cheng, D. W. Zhang and J. B. Goodenough, *Angew. Chem., Int. Ed.*, 2013, **52**, 1964–1967.
20 K. Tang, L. J. Fu, R. J. White, L. H. Yu, M.-M. Titirici, M. Antonietti and J. Maier, *Adv. Energy Mater.*, 2012, **2**, 873–877.
21 H.-G. Wang, Z. Wu, F.-L. Meng, D.-L. Ma, X.-L. Huang, L.-M. Wang and X.-B. Zhang, *ChemSusChem*, 2013, **6**, 56–60.
22 S. Yuan, X.-L. Huang, D.-L. Ma, H.-G. Wang, F.-Z. Meng and X.-B. Zhang, *Adv. Mater.*, 2014, **26**, 2273–2279.
23 H.-G. Wang, S. Yuan, D.-L. Ma, X.-L. Huang, F.-L. Meng and X.-B. Zhang, *Adv. Energy Mater.*, 2014, **4**, 1301651.
24 B. B. Lakshmi, P. K. Dorhout and C. R. Martin, *Chem. Mater.*, 1997, **9**, 857–862.
25 M. Law, J. Goldberger and P. Yang, *Annu. Rev. Mater. Res.*, 2004, **34**, 83–122.
26 M. S. Gudiksen and C. M. Lieber, *J. Am. Chem. Soc.*, 2000, **122**, 8801–8802.
27 X. Wang and Y. Li, *J. Am. Chem. Soc.*, 2002, **124**, 2880–2881.
28 V. Polshettiwar, B. Baruwati and R. S. Varma, *ACS Nano*, 2009, **3**, 728–736.
29 X. F. Wang, B. Ding, G. Sun, M. Wang and J. Y. Yu, *Prog. Mater. Sci.*, 2013, **58**, 1173–1243.
30 D. Li and Y. Xia, *Nano Lett.*, 2003, **3**, 555–560.
31 Z. M. Huang, Y. Z. Zhang, M. Kotaki and S. Ramakrishna, *Compos. Sci. Technol.*, 2003, **63**, 2223–2253.
32 A. Greiner and J. H. Wendorff, *Angew. Chem., Int. Ed.*, 2007, **46**, 5670–5703.
33 Y. H. Wang, B. Li, Y. H. Liu, L. M. Zhang, Q. H. Zuo, L. F. Shi and Z. M. Su, *Chem. Commun.*, 2009, 5868–5870.
34 D. H. Reneker and A. L. Yarin, *Polymer*, 2008, **49**, 2387–2624.
35 M. Shang, W. Z. Wang, W. Z. Yin, J. Ren, S. M. Sun and L. Zhang, *Chem. – Eur. J.*, 2010, **16**, 11412–11419.
36 H. G. Wang, Y. X. Li, L. Sun, Y. C. Li, W. Wang, S. Wang, S. F. Xu and Q. B. Yang, *J. Colloid Interface Sci.*, 2010, **350**, 396–401.
37 L. Xu, H. W. Song, B. Dong, Y. Wang, J. Chen and X. Bai, *Inorg. Chem.*, 2010, **49**, 10590–10597.
38 L. M. Li, X. M. Yin, S. Liu, Y. G. Wang, L. B. Chen and T. H. Wang, *Electrochem. Commun.*, 2010, **12**, 1383–1386.
39 C.-L. Zhang and S.-H. Yu, *Chem. Soc. Rev.*, 2014, **43**, 4423–4448.
40 H. L. Qu, S. Y. Wei and Z. H. Guo, *J. Mater. Chem. A*, 2013, **1**, 11513–11528.
41 W. Wang, Q. B. Yang, L. Sun, H. G. Wang, C. Q. Zhang, X. L. Fei, M. D. Sun and Y. X. Li, *J. Hazard. Mater.*, 2011, **194**, 185–192.
42 W. S. Chen, D. A. Huang, H. C. Chen, T. Y. Shie, C. H. Hsieh, J. D. Liao and C. Kuo, *Cryst. Growth Des.*, 2009, **9**, 4070–4077.
43 W.-E. Teo, R. Inai and S. Ramakrishna, *Sci. Technol. Adv. Mater.*, 2011, **12**, 013002.
44 M. Inagaki, Y. Yang and F. Y. Kang, *Adv. Mater.*, 2012, **24**, 2547–2566.
45 J. T. McCann, D. Li and Y. N. Xia, *J. Mater. Chem.*, 2005, **15**, 735–738.
46 J. C. Di, Y. Zhao and J. H. Yu, *J. Mater. Chem.*, 2011, **21**, 8511–8520.
47 S. Agarwal, A. Greiner and J. H. Wendorff, *Adv. Funct. Mater.*, 2009, **19**, 1–17.
48 X. F. Lu, C. Wang and Y. Wei, *Small*, 2009, **5**, 2349–2370.
49 S. Ramakrishna, K. Fujihara, W.-E. Teo, T. Yong, Z. W. Ma and R. Ramaseshan, *Mater. Today*, 2006, **9**, 40–50.
50 L. F. Zhang, A. Aboagye, A. Kelkar, C. L. Lai and H. Fong, *J. Mater. Sci.*, 2014, **49**, 463–480.
51 D. Li and Y. Xia, *Adv. Mater.*, 2004, **16**, 1151–1170.
52 D. H. Reneker, A. L. Yarin, E. Zussman and H. Xu, *Adv. Appl. Mech.*, 2007, **41–43**, 195.
53 A. L. Yarin, E. Zussman, J. H. Wendorff and A. Greiner, *J. Mater. Chem.*, 2007, **17**, 2585–2599.
54 A. L. Yarin, *Polym. Adv. Technol.*, 2011, **22**, 310–317.
55 Y. Dai, W. Liu, E. Formo, Y. Sun and Y. Xia, *Polym. Adv. Technol.*, 2011, **22**, 326–338.
56 A. Frenot and I. S. Chronakis, *Curr. Opin. Colloid Interface Sci.*, 2003, **8**, 64–75.
57 R. Ramaseshan, S. Sundarrajan, R. Jose and S. Ramakrishna, *J. Appl. Phys.*, 2007, **102**, 111101.
58 I. S. Chronakis, *J. Mater. Process. Technol.*, 2005, **167**, 283–293.
59 W. E. Teo and S. Ramakrishna, *Nanotechnology*, 2006, **17**, 89–106.
60 A. Raza, J. Y. Yu, Y. Y. Zhai, G. Sun and B. Ding, in *Electrospun Nanofibers for Energy and Environmental Applications*, ed. B. Ding and J. Y. Yu, 2014, pp. 69–89.
61 S. Cavaliere, S. Subianto, I. Savych, D. J. Jones and J. Rozière, *Energy Environ. Sci.*, 2011, **4**, 4761–4785.
62 V. Thavasi, G. Singh and S. Ramakrishna, *Energy Environ. Sci.*, 2008, **1**, 205–221.
63 Z. X. Dong, S. J. Kennedy and Y. Q. Wu, *J. Power Sources*, 2011, **196**, 4886–4904.
64 X. W. Zhang, L. W. Ji, O. Toprakci, Y. Z. Liang and M. Alcoutlabi, *Polym. Rev.*, 2011, **51**, 239–264.
65 S. Kalluri, K. H. Seng, Z. P. Guo, H. K. Liu and S. X. Dou, *RSC Adv.*, 2013, **3**, 25576–25601.
66 G. Taylor, *Proc. R. Soc. London, Ser. A*, 1969, **313**, 453–475.
67 G. Taylor, *Proc. R. Soc. London, Ser. A*, 1964, **280**, 383–397.
68 A. L. Yarin, S. Koombhongse and D. H. Reneker, *J. Appl. Phys.*, 2001, **89**, 3018–3026.
69 A. Formhals, *US Pat.*, 1975504, 1934.
70 J. Doshi and D. H. Reneker, *J. Electrost.*, 1995, **35**, 151–160.
71 D. H. Reneker and I. Chun, *Nanotechnology*, 1996, **7**, 216–223.
72 J. W. Xie, X. R. Li and Y. N. Xia, *Macromol. Rapid Commun.*, 2008, **29**, 1775–1792.
73 H. G. Wang, Q. W. Liu, Q. B. Yang, Y. C. Li, W. Wang, L. Sun, C. Q. Zhang and Y. X. Li, *J. Mater. Sci.*, 2010, **45**, 1032–1038.
74 Z. C. Sun, E. Zussman, A. L. Yarin, J. H. Wendorff and A. Greiner, *Adv. Mater.*, 2003, **15**, 1929–1932.
75 H. Dai, J. Gong, H. Kim and D. Lee, *Nanotechnology*, 2002, **13**, 674–677.
76 W. Sigmund, *J. Am. Ceram. Soc.*, 2006, **89**, 395–407.

77 H.-G. Wang, D.-L. Ma, Y. Huang and X.-B. Zhang, *Chem. – Eur. J.*, 2012, **18**, 8987–8993.
78 R. Ostermann, D. Li, Y. D. Yin, J. T. McCann and Y. N. Xia, *Nano Lett.*, 2006, **6**, 1297–1302.
79 D. Li and Y. N. Xia, *Nano Lett.*, 2004, **4**, 933–938.
80 Y. Zhao, X. Y. Cao and L. Jiang, *J. Am. Chem. Soc.*, 2007, **129**, 764–765.
81 H. Y. Chen, J. C. Di, N. Wang, H. Dong, J. Wu, Y. Zhao, J. H. Yu and L. Jiang, *Small*, 2011, **7**, 1779–1783.
82 H. Y. Chen, N. Wang, J. C. Di, Y. Zhao, Y. L. Song and L. Jiang, *Langmuir*, 2010, **26**, 11291–11296.
83 D. M. Yu, C. G. Chen, S. H. Xie, Y. Y. Liu, K. Park, X. Y. Zhou, Q. F. Zhang, J. Y. Li and G. Z. Cao, *Energy Environ. Sci.*, 2011, **4**, 858–861.
84 Z. X. Yang, G. D. Du, C. Q. Feng, S. Li, Z. X. Chen, P. Zhang, Z. P. Guo, X. B. Yu, G. N. Chen, S. Z. Huang and H. K. Liu, *Electrochim. Acta*, 2010, **55**, 5485–5491.
85 R. Sahay, P. S. Kumar, V. Aravindan, J. Sundaramurthy, W. C. Ling, S. G. Mhaisalkar, S. Ramakrishna and S. Madhavi, *J. Phys. Chem. C*, 2012, **116**, 18087–18092.
86 P. F. Teh, Y. Sharma, S. S. Pramanac and M. Srinivasan, *J. Mater. Chem.*, 2011, **21**, 14999–15008.
87 P. F. Teh, S. S. Pramana, Y. Sharma, Y. W. Ko and S. Madhavi, *ACS Appl. Mater. Interfaces*, 2013, **5**, 5461–5467.
88 L. Wang, L. J. Wu, Z. H. Li, G. T. Lei, Q. Z. Xiao and P. Zhang, *Electrochim. Acta*, 2011, **56**, 5343–5346.
89 S. H. Nam, H.-S. Shim, Y.-S. Kim, M. A. Dar, J. G. Kim and W. B. Kim, *ACS Appl. Mater. Interfaces*, 2010, **2**, 2046–2052.
90 L. Q. Mai, L. Xu, C. H. Han, X. Xu, Y. Z. Luo, S. Y. Zhao and Y. L. Zhao, *Nano Lett.*, 2010, **10**, 4750–4755.
91 Y. L. Cheah, N. Gupta, S. S. Pramana, V. Aravindan, G. Wee and M. Srinivasan, *J. Power Sources*, 2011, **196**, 6465–6472.
92 Y. L. Cheah, V. Aravindan and S. Madhavi, *ACS Appl. Mater. Interfaces*, 2012, **4**, 3270–3277.
93 A. Le Viet, M. V. Reddy, R. Jose, B. V. R. Chowdari and S. Ramakrishna, *J. Phys. Chem. C*, 2010, **114**, 664–671.
94 S. Lee, J. Ha, J. Choi, T. Song, J. W. Lee and U. Paik, *ACS Appl. Mater. Interfaces*, 2013, **5**, 11525–11529.
95 M. R. Jo, Y. S. Jung and Y.-M. Kang, *Nanoscale*, 2012, **4**, 6870–6875.
96 Y. X. Gu, D. R. Chen and X. L. Jiao, *J. Phys. Chem. B*, 2005, **109**, 17901–17906.
97 J. W. Min, C. J. Yim and W. B. Im, *ACS Appl. Mater. Interfaces*, 2013, **5**, 7765–7769.
98 C. T. Cherian, J. Sundaramurthy, M. Kalaivani, P. Ragupathy, P. S. Kumar, V. Thavasi, M. V. Reddy, C. H. Sow, S. G. Mhaisalkar, S. Ramakrishna and B. V. R. Chowdari, *J. Mater. Chem.*, 2012, **22**, 12198–12204.
99 B. Wang, J. L. Cheng, Y. P. Wu, D. Wang and D. N. He, *Electrochem. Commun.*, 2012, **23**, 5–8.
100 L. Qiao, X. H. Wang, L. Qiao, X. L. Sun, X. W. Li, Y. X. Zheng and D. Y. He, *Nanoscale*, 2013, **5**, 3037–3042.
101 L. M. Li, X. M. Yin, S. Liu, Y. G. Wang, L. B. Chen and T. H. Wang, *Electrochem. Commun.*, 2010, **12**, 1383–1386.
102 L. L. Li, S. J. Peng, J. Wang, Y. L. Cheah, P. F. Teh, Y. Ko, C. Wong and M. Srinivasan, *ACS Appl. Mater. Interfaces*, 2012, **4**, 6005–6012.
103 L. L. Li, S. J. Peng, Y. L. Cheah, J. Wang, P. F. Teh, Y. Ko, C. Wong and M. Srinivasan, *Nanoscale*, 2013, **5**, 134–138.
104 W. Luo, X. L. Hu, Y. M. Sun and Y. H. Huang, *J. Mater. Chem.*, 2012, **22**, 8916–8921.
105 H. Han, T. Song, J.-Y. Bae, L. F. Nazar, H. Kim and U. Paik, *Energy Environ. Sci.*, 2011, **4**, 4532–4536.
106 T. Yuan, B. Zhao, R. Cai, Y. K. Zhou and Z. P. Shao, *J. Mater. Chem.*, 2011, **21**, 15041–15048.
107 K. Tang, X. K. Mu, P. A. van Aken, Y. Yu and J. Maier, *Adv. Energy Mater.*, 2013, **3**, 49–53.
108 Y. X. Gu, D. R. Chen, X. L. Jiao and F. F. Liu, *J. Mater. Chem.*, 2007, **17**, 1769–1776.
109 Y. Z. Wu, P. N. Zhu, X. Zhao, M. V. Reddy, S. J. Peng, B. V. R. Chowdaric and S. Ramakrishnaad, *J. Mater. Chem. A*, 2013, **1**, 852–859.
110 W. Luo, X. L. Hu, Y. M. Sun and Y. H. Huang, *J. Mater. Chem.*, 2012, **22**, 4910–4915.
111 H. G. Wang, D. L. Ma, X. L. Huang, S. Yuan and X. B. Zhang, *Sci. Rep.*, 2012, **2**, 701.
112 Y. M. Chen, Z. G. Lu, L. M. Zhou, Y.-W. Mai and H. T. Huang, *Nanoscale*, 2012, **4**, 6800–6805.
113 Y. M. Chen, Z. G. Lu, L. M. Zhou, Y.-W. Mai and H. T. Huang, *Energy Environ. Sci.*, 2012, **5**, 7898–7902.
114 Y. Yu, L. Gu, C. B. Zhu, P. A. van Aken and J. Maier, *J. Am. Chem. Soc.*, 2009, **131**, 15984–15985.
115 Y. Yu, L. Gu, C. L. Wang, A. Dhanabalan, P. A. van Aken and J. Maier, *Angew. Chem., Int. Ed.*, 2009, **48**, 6485–6489.
116 B.-O. Jang, S.-H. Park and W.-J. Lee, *J. Alloys Compd.*, 2013, **574**, 325–330.
117 Z. X. Yang, G. D. Du, Z. P. Guo, X. B. Yu, S. Li, Z. X. Chen, P. Zhang and H. K. Liu, *Nanoscale*, 2010, **2**, 1011–1017.
118 X. S. Zhou, Z. H. Dai, S. H. Liu, J. C. Bao and Y.-G. Guo, *Adv. Mater.*, 2014, **26**, 3943.
119 D. Kim, D. Lee, J. Kim and J. Moon, *ACS Appl. Mater. Interfaces*, 2012, **4**, 5408–5415.
120 Z. X. Yang, G. D. Du, Q. Meng, Z. P. Guo, X. B. Yu, Z. X. Chen, T. L. Guo and R. Zeng, *J. Mater. Chem.*, 2012, **22**, 5848–5854.
121 X. Y. Li, Y. M. Chen, L. M. Zhou, Y.-W. Mai and H. T. Huang, *J. Mater. Chem. A*, 2014, **2**, 3875–3880.
122 P. Zhang, Z. P. Guo, Y. D. Huang, D. Z. Jia and H. K. Liu, *J. Power Sources*, 2011, **196**, 6987–6991.
123 W. Luo, X. L. Hu, Y. M. Sun and Y. H. Huang, *Phys. Chem. Chem. Phys.*, 2011, **13**, 16735–16740.
124 B. Liu, X. L. Hu, H. H. Xu, W. Luo, Y. M. Sun and Y. H. Huang, *Sci. Rep.*, 2014, **4**, 4229.
125 Y. Z. Wu, P. N. Zhu, M. V. Reddy, B. V. R. Chowdari and S. Ramakrishna, *ACS Appl. Mater. Interfaces*, 2014, **6**, 1951–1958.
126 L. Wang, Y. Yu, P. C. Chen, D. W. Zhang and C. H. Chen, *J. Power Sources*, 2008, **183**, 717–723.
127 L. Wang, C. X. Ding, L. C. Zhang, H. W. Xu, D. W. Zhang, T. Cheng and C. H. Chen, *J. Power Sources*, 2010, **195**, 5052–5056.

128 H. S. Choi, J. G. Lee, H. Y. Lee, S. W. Kim and C. R. Park, *Electrochim. Acta*, 2010, **56**, 790–796.
129 X. S. Zhou, L.-J. Wan and Y.-G. Guo, *Small*, 2013, **9**, 2684–2688.
130 B.-S. Leea, S.-B. Son, K.-M. Park, J.-H. Seo, S.-H. Lee, I.-S. Choi, K.-H. Oh and W.-R. Yu, *J. Power Sources*, 2012, **206**, 267–273.
131 T. H. Hwang, Y. M. Lee, B.-S. Kong, J.-S. Seo and J. W. Choi, *Nano Lett.*, 2012, **12**, 802–807.
132 J. Kong, W. A. Yee, Y. Wei, L. Yang, J. M. Ang, S. L. Phua, S. Y. Wong, R. Zhou, Y. Dong, X. Li and X. Lu, *Nanoscale*, 2013, **5**, 2967–2973.
133 Q. L. Wu, T. Tran, W. Q. Lu and J. Wu, *J. Power Sources*, 2014, **258**, 39–45.
134 Z. X. Yang, Q. Meng, Z. P. Guo, X. B. Yu, T. L. Guo and R. Zeng, *Energy*, 2013, **55**, 925–932.
135 B. K. Guo, Y. Li, Y. F. Yao, Z. Lin, L. W. Ji, G. J. Xu, Y. Z. Liang, Q. Shi and X. W. Zhang, *Solid State Ionics*, 2011, **204–205**, 61–65.
136 Q. Q. Chen, X. C. Qiao, C. Peng, T. T. Zhang, Y. B. Wang and X. Y. Wang, *Electrochim. Acta*, 2012, **78**, 40–48.
137 C. B. Zhu, Y. Yu, L. Gu, K. Weichert and J. Maier, *Angew. Chem., Int. Ed.*, 2011, **50**, 1–6.
138 L. W. Ji and X. W. Zhang, *Nanotechnology*, 2009, **20**, 155705.
139 L. W. Ji, Y. F. Yao, O. Toprakci, Z. Lin, Y. Z. Liang, Q. Shi, A. J. Medford, C. R. Millns and X. W. Zhang, *J. Power Sources*, 2010, **195**, 2050–2056.
140 L. W. Ji, Z. Lin, A. J. Medford and X. W. Zhang, *Carbon*, 2009, **47**, 3346–3354.
141 L. W. Ji and X. W. Zhang, *Electrochem. Commun.*, 2009, **11**, 684–687.
142 L. W. Ji, Z. Lin, R. Zhou, Q. Shi, O. Toprakci, A. J. Medford, C. R. Millns and X. W. Zhang, *Electrochim. Acta*, 2010, **55**, 1605–1611.
143 L. W. Ji, Z. Lin, A. J. Medford and X. W. Zhang, *Chem. – Eur. J.*, 2009, **15**, 10718–10722.
144 L. W. Ji, Z. Lin, B. K. Guo, A. J. Medford and X. W. Zhang, *Chem. – Eur. J.*, 2010, **16**, 11543–11548.
145 C. A. Bonino, L. W. Ji, Z. Lin, O. Toprakci, X. W. Zhang and S. A. Khan, *ACS Appl. Mater. Interfaces*, 2011, **3**, 2534–2542.
146 Z. Lin, L. W. Ji, M. D. Woodroof and X. W. Zhang, *J. Power Sources*, 2010, **195**, 5025–5031.
147 L. W. Ji and X. W. Zhang, *Electrochem. Commun.*, 2009, **11**, 795–798.
148 L. W. Ji, A. J. Medford and X. W. Zhang, *J. Mater. Chem.*, 2009, **19**, 5593–5601.
149 L. W. Ji, K.-H. Jung, A. J. Medford and X. W. Zhang, *J. Mater. Chem.*, 2009, **19**, 4992–4997.
150 L. W. Ji and X. W. Zhang, *Electrochem. Commun.*, 2009, **11**, 1146–1149.
151 L. W. Ji and X. W. Zhang, *Energy Environ. Sci.*, 2010, **3**, 124–129.
152 O. Toprakci, L. W. Ji, Z. Lin, H. A. K. Toprakci and X. W. Zhang, *J. Power Sources*, 2011, **196**, 7692–7699.
153 O. Toprakci, H. A. K. Toprakci, L. W. Ji, G. J. Xu, Z. Lin and X. W. Zhang, *ACS Appl. Mater. Interfaces*, 2012, **4**, 1273–1280.
154 H. Wu, G. Y. Zheng, N. Liu, T. J. Carney, Y. Yang and Y. Cui, *Nano Lett.*, 2012, **12**, 904–909.
155 C. Kim, K. S. Yang, M. Kojima, K. Yoshida, Y. J. Kim, Y. A. Kim and M. Endo, *Adv. Funct. Mater.*, 2006, **16**, 2393–2397.
156 Y. H. Yu, Q. Yang, D. H. Teng, X. P. Yang and S. Ryu, *Electrochem. Commun.*, 2010, **12**, 1187–1190.
157 X. J. Yang, D. H. Teng, B. X. Liu, Y. H. Yu and X. P. Yang, *Electrochem. Commun.*, 2011, **13**, 1098–1101.
158 S.-X. Wang, L. P. Yang, L. P. Stubbs, X. Li and C. B. He, *ACS Appl. Mater. Interfaces*, 2013, **5**, 12275–12282.
159 L. Zou, L. Gan, F. Y. Kang, M. X. Wang, W. C. Shen and Z. H. Huang, *J. Power Sources*, 2010, **195**, 1216–1220.
160 W. H. Li, Z. H. Yang, J. X. Cheng, X. W. Zhong, L. Gu and Y. Yu, *Nanoscale*, 2014, **6**, 4532–4537.
161 J. H. Kong, Z. L. Liu, Z. C. Yang, H. R. Tan, S. X. Xiong, S. Y. Wong, X. Li and X. H. Lu, *Nanoscale*, 2012, **4**, 525–530.
162 L. Zou, L. Gan, R. T. Lv, M. X. Wang, Z.-h. Huang, F. Y. Kang and W. C. Shen, *Carbon*, 2011, **49**, 89–95.
163 B. Zhang, Y. Yu, Z. D. Huang, Y.-B. He, D. Jang, W.-S. Yoon, Y.-W. Mai, F. Y. Kang and J.-K. Kim, *Energy Environ. Sci.*, 2012, **5**, 9895–9902.
164 G. Yang, Y. H. Li, H. M. Ji, H. Y. Wang, P. Gao, L. Wang, H. D. Liu, J. Pinto and X. F. Jiang, *J. Power Sources*, 2012, **216**, 353–362.
165 M. Zhang, E. Uchaker, S. Hu, Q. F. Zhang, T. H. Wang, G. Z. Cao and J. Y. Li, *Nanoscale*, 2013, **5**, 12342–12349.
166 C. Y. Zhao, J. H. Kong, X. Y. Yao, X. S. Tang, Y. L. Dong, S. L. Phua and X. H. Lu, *ACS Appl. Mater. Interfaces*, 2014, **6**, 6392–6398.
167 R. von Hagen, H. Lorrmann, K.-C. Möller and S. Mathur, *Adv. Energy Mater.*, 2012, **2**, 553–559.
168 M. S. Whittingham, *J. Electrochem. Soc.*, 1976, **123**, 315–320.
169 D. M. Yu, C. G. Chen, S. H. Xie, Y. Y. Liu, K. Park, X. Y. Zhou, Q. F. Zhang, J. Y. Li and G. Z. Cao, *Energy Environ. Sci.*, 2011, **4**, 858–861.
170 N. A. Chernova, M. Roppolo, A. C. Dillon and M. S. Whittingham, *J. Mater. Chem.*, 2009, **19**, 2526–2552.
171 D. W. Liu and G. Z. Cao, *Energy Environ. Sci.*, 2010, **3**, 1218–1237.
172 W. Hu, X.-B. Zhang, Y.-L. Cheng, C.-Y. Wu, F. Cao and L.-M. Wang, *ChemSusChem*, 2011, **4**, 1091–1094.
173 W. Hu, X.-B. Zhang, Y.-L. Cheng, Y.-M. Wu and L.-M. Wang, *Chem. Commun.*, 2011, **47**, 5250–5252.
174 M. Giorgetti, M. Berrettoni and W. H. Smyrl, *Chem. Mater.*, 2007, **19**, 5991–6000.
175 Y. Gu, D. Chen, X. Jiao and F. Liu, *J. Mater. Chem.*, 2006, **16**, 4361–4366.
176 L. Cheng, J. Yan, G. N. Zhu, J. Y. Luo, C. X. Wang and Y. Y. Xia, *J. Mater. Chem.*, 2010, **20**, 595–601.
177 E. M. Sorensen, S. J. Barry, H. K. Jung, J. R. Rondinelli, J. T. Vaughey and K. R. Poeppelmeier, *Chem. Mater.*, 2006, **18**, 482–489.
178 S. C. Lee, S. M. Lee, J. W. Lee, J. B. Lee, S. M. Lee, S. S. Han, H. C. Lee and J. H. Kim, *J. Phys. Chem. C*, 2009, **113**, 18420–18423.

179 G. J. Wang, J. Gao, L. J. Fu, N. H. Zhao, Y. P. Wu and T. Takamura, *J. Power Sources*, 2007, **174**, 1109–1112.
180 N. C. Li, C. J. Patrissi, G. L. Che and C. R. Martin, *J. Electrochem. Soc.*, 2000, **147**, 2044–2049.
181 P. R. Bueno and E. R. Leite, *J. Phys. Chem. B*, 2003, **107**, 8868–8877.
182 Y. Ou, J. J. Wen, H. P. Xu, S. H. Xie and J. Y. Li, *J. Phys. Chem. Solids*, 2013, **74**, 322–327.
183 Z. H. Wen, Q. Wang, Q. Zhang and J. H. Li, *Adv. Funct. Mater.*, 2007, **17**, 2772–2778.
184 Y. Wang, J. Y. Lee and H. C. Zeng, *Chem. Mater.*, 2005, **17**, 3899–3903.
185 A. Yu and R. Frech, *J. Power Sources*, 2002, **104**, 97–100.
186 Y. Wang and J. Y. Lee, *J. Phys. Chem. B*, 2004, **108**, 17832–17837.
187 J. K. Shon, H. Kim, S. S. Kong, S. H. Hwang, T. H. Han, J. M. Kim, C. Pak, S. Doo and H. Chang, *J. Mater. Chem.*, 2009, **19**, 6727–6732.
188 G. T.-K. Fey, P. Muralidharan, C.-Z. Lu and Y.-D. Cho, *Solid State Ionics*, 2005, **176**, 2759–2767.
189 H. Zhao, L. Gao, W. Qiu and X. Zhang, *J. Power Sources*, 2004, **132**, 195–200.
190 T. Fang, J.-G. Duh and S.-R. Sheen, *J. Electrochem. Soc.*, 2005, **152**, A1701–A1706.
191 P. N. Zhu, Y. Z. Wu, M. V. Reddy, A. S. Nair, B. V. R. Chowdari and S. Ramakrishna, *RSC Adv.*, 2012, **2**, 531–537.
192 X. Zhang, P. S. Kumar, V. Aravindan, H. H. Liu, J. Sundaramurthy, S. G. Mhaisalkar, H. M. Duong, S. Ramakrishna and S. Madhavi, *J. Phys. Chem. C*, 2012, **116**, 14780–14788.
193 N. Zhua, W. Liu, M. Q. Xue, Z. Xie, D. Zhao, M. N. Zhang, J. T. Chen and T. B. Cao, *Electrochim. Acta*, 2010, **55**, 5813–5818.
194 E. Hosono, Y. G. Wang, N. Kida, M. Enomoto, N. Kojima, M. Okubo, H. Matsuda, Y. Saito, T. Kudo, I. Honma and H. S. Zhou, *ACS Appl. Mater. Interfaces*, 2010, **2**, 212–218.
195 G. M. Zhou, F. Li and H.-M. Cheng, *Energy Environ. Sci.*, 2014, **7**, 1307–1338.
196 L. Li, Z. Wu, S. Yuan and X.-B. Zhang, *Energy Environ. Sci.*, 2014, **7**, 2101–2122.
197 K. Saravanan, C. W. Mason, A. Rudola, K. H. Wong and P. Balaya, *Adv. Energy Mater.*, 2013, **3**, 444–450.
198 H. Kim, R. A. Shakoor, C. Park, S. Y. Lim, J.-S. Kim, Y. N. Jo, W. Cho, K. Miyasaka, R. Kahraman, Y. Jung and J. W. Choi, *Adv. Funct. Mater.*, 2013, **23**, 1147–1155.
199 S. Tepavcevic, H. Xiong, V. R. Stamenkovic, X. B. Zuo, M. Balasubramanian, V. B. Prakapenka, C. S. Johnson and T. Rajh, *ACS Nano*, 2012, **6**, 530–538.
200 D. Kim, S.-H. Kang, M. Slater, S. Rood, J. T. Vaughey, N. Karan, M. Balasubramanian and C. S. Johnson, *Adv. Energy Mater.*, 2011, **1**, 333–336.
201 M. Zhou, J. F. Qian, X. P. Ai and H. X. i Yang, *Adv. Mater.*, 2011, **23**, 4913–4917.
202 Y. L. Cao, L. F. Xiao, M. L. Sushko, W. Wang, B. Schwenzer, J. Xiao, Z. M. Nie, L. V. Saraf, Z. G. Yang and J. Liu, *Nano Lett.*, 2012, **12**, 3783–3787.
203 Y. Park, D.-S. Shin, S. H. Woo, N. S. Choi, K. H. Shin, S. M. Oh, K. T. Lee and S. Y. Hong, *Adv. Mater.*, 2012, **24**, 3562–3567.
204 L. Zhao, J. M. Zhao, Y.-S. Hu, H. Li, Z. B. Zhou, M. Armand and L. Q. Chen, *Adv. Energy Mater.*, 2012, **2**, 962–965.
205 A. Abouimrane, W. Weng, H. Eltayeb, Y. J. Cui, J. Niklas, O. Poluektov and K. Amine, *Energy Environ. Sci.*, 2012, **5**, 9632–9638.
206 K. Sakaushi, E. Hosono, G. Nickerl, T. Gemming, H. S. Zhou, S. Kaskel and J. Eckert, *Nat. Commun.*, 2013, **4**, 1485.
207 J. F. Qian, X. Y. Wu, Y. L. Cao, X. P. Ai and H. X. Yang, *Angew. Chem., Int. Ed.*, 2013, **52**, 4633–4636.
208 H. L. Pan, X. Lu, X. Q. Yu, Y.-S. Hu, H. Li, X.-Q. Yang and L. Q. Chen, *Adv. Energy Mater.*, 2013, **3**, 1186–1194.
209 Y. H. Liu, Y. H. Xu, Y. J. Zhu, J. N. Culver, C. A. Lundgren, K. Xu and C. S. Wang, *ACS Nano*, 2013, **7**, 3627–3634.
210 Y. H. Xu, Y. J. Zhu, Y. H. Liu and C. S. Wang, *Adv. Energy Mater.*, 2013, **3**, 128–133.
211 Z. L. Jian, C. C. Yuan, W. Z. Han, X. Lu, L. Gu, X. K. Xi, Y.-S. Hu, H. Li, W. Chen, D. F. Chen, Y. Ikuhara and L. Q. Chen, *Adv. Funct. Mater.*, 2014, **24**, 4265–4272.
212 S. W. Wang, L. J. Wang, Z. Q. Zhu, Z. Hu, Q. Zhao and J. Chen, *Angew. Chem., Int. Ed.*, 2014, **53**, 5892–5896.
213 J. F. Qian, Y. Xiong, Y. L. Cao, X. P. Ai and H. X. Yang, *Nano Lett.*, 2014, **14**, 1865–1869.
214 D. Y. W. Yu, P. V. Prikhodchenko, C. W. Mason, S. K. Batabyal, J. Gun, S. Sladkevich, A. G. Medvedev and O. Lev, *Nat. Commun.*, 2014, **4**, 2922.
215 T. Q. Chen, Y. Liu, L. K. Pan, T. Lu, Y. F. Yao, Z. Sun, D. H. C. Chua and Q. Chen, *J. Mater. Chem. A*, 2014, **2**, 4117–4121.
216 L. Wu, X. H. Hu, J. F. Qian, F. Pei, F. Y. Wu, R. J. Mao, X. P. Ai, H. X. Yang and Y. L. Cao, *Energy Environ. Sci.*, 2014, **7**, 323–328.
217 L. W. Ji, M. Gu, Y. Y. Shao, X. L. Li, M. H. Engelhard, B. W. Arey, W. Wang, Z. M. Nie, J. Xiao, C. M. Wang, J.-G. Zhang and J. Liu, *Adv. Mater.*, 2014, **26**, 2901–2908.
218 C. B. Zhu, X. K. Mu, P. A. van Aken, Y. Yu and J. Maier, *Angew. Chem., Int. Ed.*, 2014, **53**, 2152–2156.
219 J. Liu, K. Tang, K. P. Song, P. A. van Aken, Y. Yu and J. Maier, *Phys. Chem. Chem. Phys.*, 2013, **15**, 20813–20818.
220 J. Liu, K. Tang, K. P. Song, P. A. van Aken, Y. Yu and J. Maier, *Nanoscale*, 2014, **6**, 5081–5086.
221 T. H. Hwang, D. S. Jung, J.-S. Kim, B. G. Kim and J. W. Choi, *Nano Lett.*, 2013, **13**, 4532–4538.
222 W. H. Li, L. C. Zeng, Z. Z. Yang, L. Gu, J. Q. Wang, X. W. Liu, J. X. Cheng and Y. Yu, *Nanoscale*, 2014, **6**, 693–698.
223 Y. J. Zhu, X. G. Han, Y. H. Xu, Y. H. Liu, S. Y. Zheng, K. Xu, L. B. Hu and C. S. Wang, *ACS Nano*, 2013, **7**, 6378–6386.
224 P. Ge and M. Fouletier, *Solid State Ionics*, 1988, **28**, 1172–1175.
225 D. A. Stevens and J. R. Dahn, *J. Electrochem. Soc.*, 2001, **148**, A803–A811.
226 M. M. Doeff, Y. Ma, S. J. Visco and L. C. de Jonghe, *J. Electrochem. Soc.*, 1993, **140**, L169–L170.

227 R. Alcántara, J. M. J. Mateos and J. L. Tirado, *J. Electrochem. Soc.*, 2002, **149**, A201–A205.
228 R. Alcántara, J. M. Jiménez-Mateo, P. Lavela and J. L. Tirado, *Electrochem. Commun.*, 2001, **3**, 639–642.
229 D. Stevens and J. Dahn, *J. Electrochem. Soc.*, 2000, **147**, 1271–1273.
230 P. Thomas and D. Billaud, *Electrochim. Acta*, 2001, **46**, 3359–3366.
231 S. Wenzel, T. Hara, J. Janek and P. Adelhelm, *Energy Environ. Sci.*, 2011, **4**, 3342–3345.
232 M. K. Datta, R. Epur, P. Saha, K. Kadakia, S. K. Park and P. N. Kumta, *J. Power Sources*, 2013, **225**, 316–322.
233 H. Zhu, Z. Jia, Y. Chen, N. J. Weadock, J. Wan, O. Vaaland, X. Han, T. Li and L. Hu, *Nano Lett.*, 2013, **13**, 3093–3100.
234 J. Qian, Y. Chen, L. Wu, Y. Cao, X. Ai and H. Yang, *Chem. Commun.*, 2012, **48**, 7070–7072.
235 A. Darwiche, C. Marino, M. T. Sougrati, B. Fraisse, L. Stievano and L. Monconduit, *J. Am. Chem. Soc.*, 2012, **134**, 20805–20811.
236 V. L. Chevrier and G. Ceder, *J. Electrochem. Soc.*, 2011, **158**, A1011–A1014.
237 A. Darwiche, M. T. Sougrati, B. Fraisse, L. Stievano and L. Monconduit, *Electrochem. Commun.*, 2013, **32**, 18–21.
238 L. Xiao, Y. Cao, J. Xiao, W. Wang, L. Kovarik, Z. Nie and J. Liu, *Chem. Commun.*, 2012, **48**, 3321–3323.
239 J. Shu, H. Li, R. Yang, Y. Shi and X. Huang, *Electrochem. Commun.*, 2006, **8**, 51–54.
240 C. K. Chan, R. Ruffo, S. S. Hong and Y. Cui, *J. Power Sources*, 2009, **189**, 1132–1140.
241 J. T. Lee, N. Nitta, J. Benson, A. Magasinski, T. F. Fuller and G. Yushin, *Carbon*, 2013, **52**, 388–397.
242 M. Herstedt, A. M. Andersson, H. Rensmo, H. Siegbahn and K. Edström, *Electrochim. Acta*, 2004, **49**, 4939–4947.
243 V. Etacheri, O. Haik, Y. Goffer, G. A. Roberts, I. C. Stefan, R. Fasching and D. Aurbach, *Langmuir*, 2012, **28**, 965–976.
244 D. Y. W. Yu, P. V. Prikhodchenko, C. W. Mason, S. K. Batabyal, J. Gun, S. Sladkevich, A. G. Medvedev and O. Lev, *Nat. Commun.*, 2014, **4**, 2922.
245 L. David, R. Bhandavat and G. Singh, *ACS Nano*, 2014, **8**, 1759–1770.
246 Q. Pan, J. Xie, T. J. Zhu, G. S. Cao, X. B. Zhao and S. C. Zhang, *Inorg. Chem.*, 2014, **53**, 3511–3518.
247 B. H. Qu, C. Z. Ma, G. Ji, C. H. Xu, J. Xu, Y. S. Meng, T. H. Wang and J. Y. Lee, *Adv. Mater.*, 2014, **26**, 3854–3859.
248 D. Li, Y. Wang and Y. Xia, *Nano Lett.*, 2003, **3**, 1167–1171.
249 B. Sundaray, V. Subramanian, T. S. Natarajan, R.-Z. Xiang, C.-C. Chang and W.-S. Fann, *Appl. Phys. Lett.*, 2004, **84**, 1222–1224.
250 B. Sundaray, V. Subramanian, T. S. Natarajan and K. Krishnamurthy, *Appl. Phys. Lett.*, 2006, **88**, 143114.
251 N. Q. Zhan, Y. X. Li, C. Q. Zhang, Y. Song, H. G. Wang, L. Sun, Q. B. Yang and X. Hong, *J. Colloid Interface Sci.*, 2010, **345**, 491–495.
252 C. Q. Zhang, Y. P. Li, W. Wang, N. Q. Zhan, N. Xiao, S. Wang, Y. X. Li and Q. B. Yang, *Eur. Polym. J.*, 2011, **47**, 2228–2233.
253 Z. S. Wu, W. Ren, L. Xu, F. Li and H. M. Cheng, *ACS Nano*, 2011, **5**, 5463–5471.
254 F. Su, C. K. Poh, J. S. Chen, G. Xu, D. Wang, Q. Li, J. Lin and X. W. Lou, *Energy Environ. Sci.*, 2011, **4**, 717–724.
255 L. Qie, W. M. Chen, Z. H. Wang, Q. G. Shao, X. Li, L. X. Yuan, X. L. Hu, W. X. Zhang and Y. H. Huang, *Adv. Mater.*, 2012, **24**, 2047–2050.
256 Z. S. Wu, S. B. Yang, Y. Sun, K. Parvez, X. L. Feng and K. Mullen, *J. Am. Chem. Soc.*, 2012, **134**, 9082–9085.